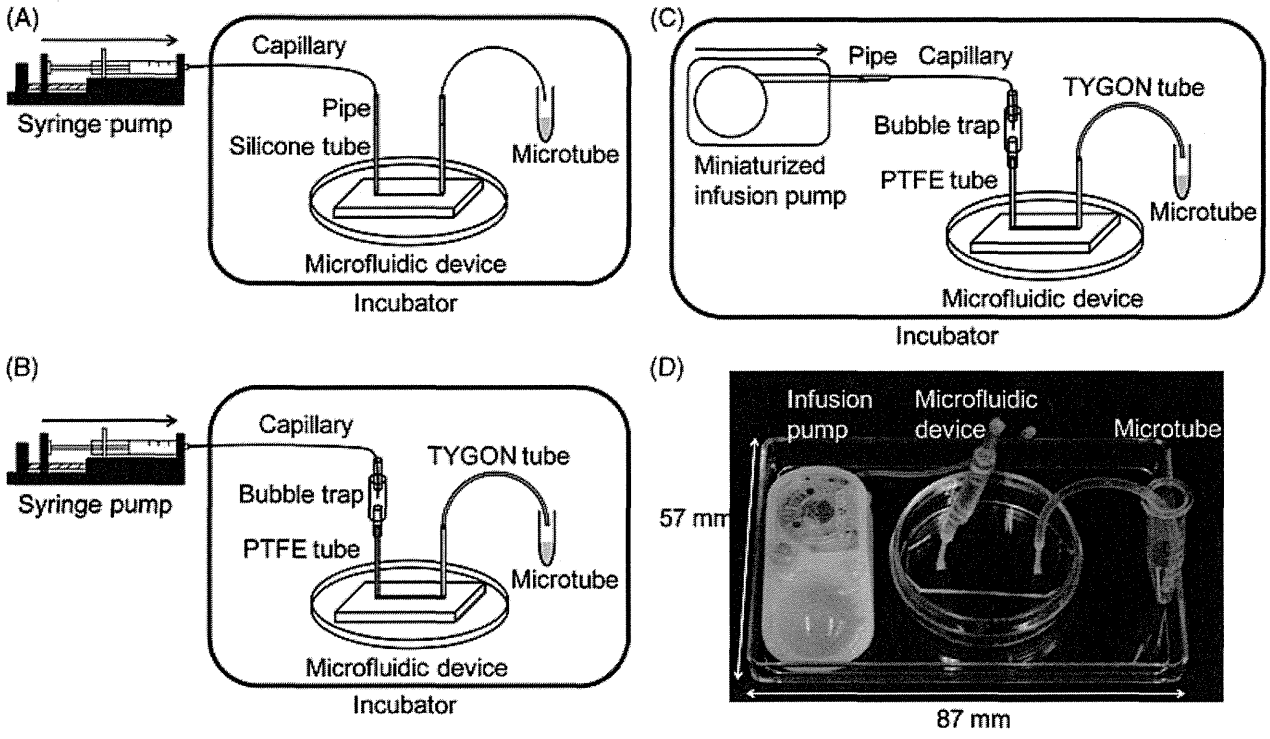

Figure 1. Microfluidic cell culture systems. (A–C) Schematic illustrations of microfluidic cell culture system. (A) A system with a syringe pump. (B) A system with a syringe pump and a bubble trap. (C) A palmtop-sized culture system with a miniaturized infusion pump and a bubble trap. (D) Photograph of the palmtop-sized microfluidic cell culture system.

The other PTFE tube on the microfluidic device was also connected to a TYGON tube. In the palmtop-sized microfluidic cell culture system shown in Fig. 1C, a miniaturized infusion pump (SMP101-L, Primetech, Tokyo, Japan) was used instead of the syringe pump shown in Fig. 1B. The components of the systems were glued with epoxy adhesive as required.

2.4 Cell culture in a microchannel

All the tubes, pipes, and capillaries used in this study were sterilized in an autoclave at 121°C for 20 min. Medium for cell culture was incubated in an incubator for 30 min prior to experiments to equilibrate the concentration of CO_2 in the medium with that in the incubator. Microfluidic devices were degassed in a vacuum desiccator (PC-150K, Sanplatec, Osaka, Japan) connected to a vacuum pump (DAP-6D, Ulvac, Kanagawa, Japan) at 10 kPa for 30 min to prevent air bubbles remaining in the microchannels [39].

A suspension of cells was prepared at a cell concentration of 5×10^6 cells mL^{-1} and then introduced into a microchannel manually or by a syringe pump. Capillaries were then pinched by clips to stop the flow in the microchannel. The microfluidic device was wrapped with a wet lint-free wiper (BEMCOT™ M-1, Asahi Kasei, Tokyo, Japan) in plastic wrap to humidify the device. The microfluidic device was incubated at 37°C under an atmosphere of 5% CO_2 and 95% air for 5 h to allow cells to adhere to the bottom of the channel. The medium was then infused into the channel at 6.0 μL h^{-1} by the syringe pump placed outside the incubator (Fig. 1A and B) or the miniaturized infusion pump placed inside the incubator (Fig. 1C).

Shear stress during the culture was estimated as follows. Time-averaged shear stress τ in a rectangular microchannel is written as [40]:

$$\tau = \frac{2\mu Q}{wh^2}\left(\frac{m+1}{m}\right)(n+1) \quad (1)$$

where μ is the viscosity of the medium, Q is the volume flow rate, h is the height of the microchannel, w is the width of the microchannel, and m and n are empirical constants, with $m = 1.7 + 0.5(h/w)^{-1.4}$ and $n = 2$ for aspect ratios $h/w < 1/3$. As described previously [29], μ was assumed to be the same as that of water at 37°C, and estimated to be 7.0×10^{-3} g cm^{-1} s^{-1}. Using the μ value, a h of 67 μm, w of 300 μm, Q of 6.0 μL h^{-1} and Eq. 1, we obtained 0.061 dyn cm^{-2} as the time-averaged shear stress in the microchannel.

The miniaturized pump creates intermittent flow because of its peristaltic mechanism. Therefore, we measured instantaneous volume flow rate in a separate experiment and estimated shear stress (see Supporting information). The maximum instantaneous volume flow rate was 16.3 μL h^{-1}, and we obtained 0.17 dyn cm^{-2} as the maximum instantaneous shear stress.

The cultured cells were observed using an inverted microscope (IX71, Olympus, Tokyo, Japan) equipped with a CCD camera (Rolera XR, QImaging, Surrey, BC, Canada).

Phase-contrast images of HMEC-1 and HUVEC were taken at 102 h and 50 h, respectively, after introduction of the cell suspension.

2.5 Evaluation of proliferation rate

In macroscale experiments, 250 μL of a HMEC-1 suspension at a cell concentration of 4×10^5 cells mL^{-1} was added to 5 mL of fresh medium in a cell culture flask, and the cells were cultured under a static condition. In microscale experiments, microfluidic devices were degassed as described in the previous section. The medium was introduced into the microchannel at 1200 μL h^{-1} by a syringe pump. A suspension of HMEC-1 at a cell concentration of 5×10^6 cells mL^{-1} was then introduced into the microchannel at 600 μL h^{-1}, and the microfluidic devices were incubated in the CO_2 incubator for 4 h. Finally, the medium was pumped into the channel by the syringe pump or a miniaturized infusion pump at 6.0 μL h^{-1}. The cultured cells were observed as described in the previous section. Phase-contrast images of HMEC-1 were taken at 4 h (just before pumping medium), 28 h, 53 h, 83 h, 102 h, and 129 h after introduction of the cell suspension.

2.6 Evaluation of orientation

The orientation of HUVEC was evaluated in accordance with details provided in the literature [16]. Briefly, the angle of orientation was defined as the angle between the long axis of the cell and the direction of flow. Therefore, the angle of a cell that is completely oriented parallel to the microchannel is regarded as 0°, whereas the angle of a cell that is completely oriented perpendicular to the microchannel is regarded as 90°.

2.7 Immunofluorescent staining

HUVEC cultured in a microchannel were immunostained for Claudin-5, a transmembrane protein that is involved in tight junctions between endothelial cells [41]. After 50 h in culture, HUVEC was fixed with methanol, rinsed with PBS, blocked with PBS containing 1% BSA (Wako Pure Chemical Industries, Osaka, Japan) for 30 min, rinsed with PBS three times for 5 min each, and then reacted with 10 μg mL^{-1} anti-Claudin-5 antibody (ab53765, abcam, Cambridge, UK) for 12 h at 4°C. The cells were then rinsed with PBS three times for 5 min each, reacted with 6.7 μg mL^{-1} Alexa Fluor™ 555 goat anti-rabbit IgG antibody (A-21429, Invitrogen) for 30 min at room temperature, and rinsed with PBS three times for 5 min each. The nuclei of cells were counterstained with Dapi-Fluoromount-G™ (SouthernBiotech, Birmingham, AL, USA). Fluorescence images were taken using the same microscope described in Section 2.4 equipped with a 100-W high-pressure mercury lamp, a 20× objective lens (NA 0.40), and a cooled CCD camera (ORCA-R2, Hamamatsu Photonics, Hamamatsu, Japan). For Claudin-5 observation, a dichroic mirror block (U-MWIG3, excitation 530–550 nm and emission >575 nm) was used. For the observation of nuclei, another dichroic mirror block (U-MNUA2, excitation 360–370 nm and emission 420–460 nm) was used. The images were processed using image analysis software (Image J 1.45f, National Institutes of Health, MD, USA).

3 Results and discussions

3.1 Palmtop-sized microfluidic cell culture system

Figure 1D shows a photograph of the palmtop-sized microfluidic cell culture system. The system consists of a miniaturized infusion pump, a microfluidic device, a microtube, and tubes and capillaries that connect the components of the system. A reservoir (900 μL) of culture medium and an electrical control circuit are integrated into the pump (44 mm length, 22 mm width, 10 mm height, 7 g weight). The reservoir is connected to a rubber tube in the pump, and the tube is pushed by seven pins in the pump in a sequential manner. Therefore, the medium is pumped in a peristaltic manner. The range of volume flow rate is 1.0~30.0 μL h^{-1}. The pump is programmable, and we can configure up to ten discrete infusion steps. The pump is commercially available at low cost (¥25 000 per pump). The pump is disposable since it is an implantable pump for small laboratory animals, but should be reusable in our system if it is sterilized with appropriate solutions (e.g., 70% ethanol). In addition, the pump is powered by an internal battery, and therefore no cables or tubes are required from outside the system. As a result, the footprint of the whole system was reduced to 87 × 57 mm, which is, to the best of our knowledge, the smallest integrated cell culture system. The system can be placed in an incubator for culture and on a microscope for observation without detaching any electrical or fluidic connections from the system.

3.2 Culture of endothelial cells

Figure 2 shows typical images of HMEC-1 and HUVEC cultured in a microchannel. Both types of cells reached confluence in the microchannel, whether the channel was perfused by a syringe pump (Fig. 2A and C) or a miniaturized infusion pump (Fig. 2B and D). Therefore, both cell lines and normal cells reached confluence in the palmtop-sized cell culture system. HMEC-1 was not oriented to a specific direction, whereas HUVEC was oriented to the direction of the channel. The orientation of HUVEC is further discussed in Section 3.4.

We also observed air bubbles in the systems in some experiments. HMEC-1 was successfully cultured in the system shown in Fig. 1A. In contrast, when HUVEC was cultured in the system shown in Fig. 1A, air bubbles flowed into the channel and detached the cells from the surface of the channel (data not shown). Such issues were solved by placing

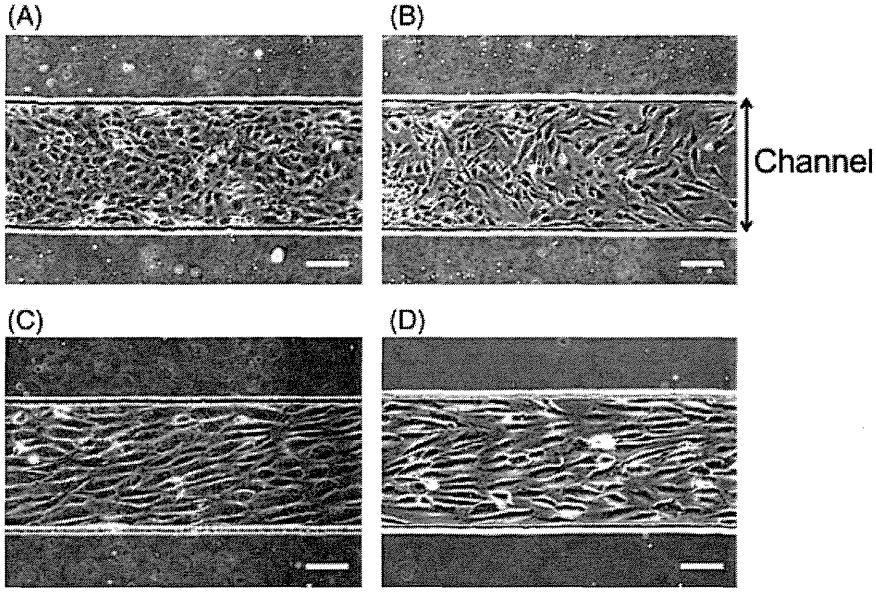

Figure 2. Phase-contrast images of (A, B) HMEC-1 and (C, D) HUVEC cultured in a microchannel. The cells were cultured with (A, C) a syringe pump and (B, D) a miniaturized infusion pump. Scale bar: 100 μm.

the bubble trap at the upstream point of the microchannel, as shown in Fig. 1B and C.

3.3 Growth rate of endothelial cells

Figure 3 shows the growth curve of HMEC-1 under three different culture procedures: static culture in a culture flask, perfusion culture in a microchannel with a syringe pump, and perfusion culture in a microchannel with a miniaturized infusion pump. In a culture flask, the cell density was 96 ± 28 cells mm^{-2} at the culture time of 4 h. The density then increased with time, and reached (1.4 ± 0.3) × 10^3 cells mm^{-2} at 102 h. Afterward, the density was almost constant, which meant the cells reached confluence at 102 h. In a microchannel perfused by a syringe pump, the cell density was (1.4 ± 0.4) × 10^2 cells mm^{-2} at 4 h and reached (1.1 ± 0.1) × 10^3 cells mm^{-2} at 102 h. In a microchannel perfused by a miniaturized infusion pump, the cell density was (1.5 ± 0.4) × 10^2 cells mm^{-2} at 4 h and reached (1.2 ± 0.1) × 10^3 cells mm^{-2} at 102 h. Clearly, the cell densities at the culture time of 4 h and 102 h in the aforementioned culture procedures were almost the same, and hence the proliferation rates of cells were also the same. Therefore, HMEC-1 cultured with the miniaturized infusion pump proliferated in a way similar to cells cultured with the syringe pump and in a culture flask.

3.4 Orientation

Figure 4 shows a histogram of the orientation angle of HUVEC under the different culture procedures. Under static culture in a culture flask, the orientation angle of HUVEC was random: the averaged orientation angle was 43.3 ± 25.1°,

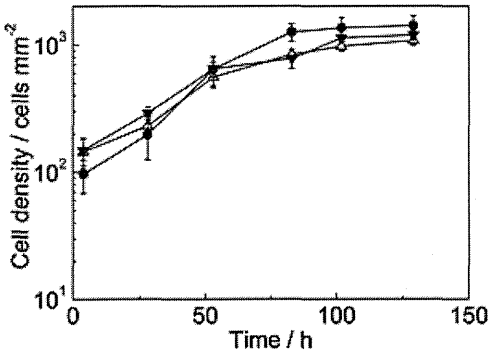

Figure 3. Growth curve of HMEC-1 under three different culture procedures: static culture in a culture flask (filled circles), perfusion culture in a microchannel with a syringe pump (open triangles), and perfusion culture in a microchannel with a miniaturized infusion pump (filled inverted triangles). The error bars indicate ±1SD of three experiments.

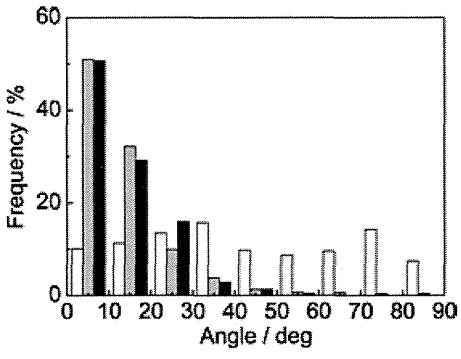

Figure 4. Histogram of orientation angle of HUVEC under three different culture procedures: static culture in a culture flask (white), perfusion culture in a microchannel with a syringe pump (gray), and perfusion culture in a microchannel with a miniaturized infusion pump (black). Culture time: 50 h. Data were taken from three experiments.

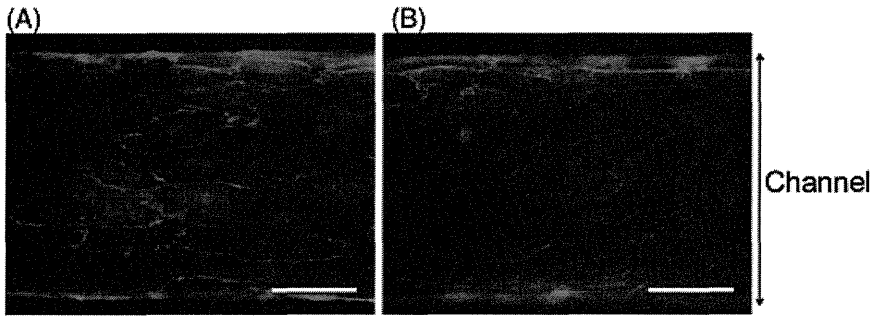

Figure 5. Immunofluorescence micrographs of HUVEC in a microchannel. Cells were immunostained for Claudin-5 (red, a marker of tight junctions). Nuclei of cells were counterstained with Dapi-Fluoromount-G (blue). (A) HUVEC cultured with a syringe pump. (B) HUVEC cultured with a miniaturized infusion pump. Scale bar: 100 μm.

which is close to the theoretical value of the averaged orientation angle for randomly oriented cells (45°). In contrast, the orientation angles of HUVEC cultured in microchannels were around zero: the averaged orientation angle of HUVEC cultured with a syringe pump and with a miniaturized infusion pump was 12.4 ± 12.0° and 12.1 ± 9.6°, respectively. Therefore, HUVEC was oriented to the direction along the channel. This result is consistent with previous reports concerning the orientation of HUVEC under continuous flow in a microchannel [13, 15].

3.5 Tight junctions

Tight junctions are a type of the intercellular junction, which represent the major transport pathway across the endothelium [42]. The presence of tight junctions between endothelial cells cultured in a microchannel has been demonstrated by TEER measurement [24]. However, the presence of tight junction proteins at the junctions has not been confirmed. Figure 5 shows immunofluorescence images of HUVEC in a microchannel. Claudin-5, the major transmembrane component of endothelial tight junctions, was localized along the cell peripheries as previously reported [43, 44], regardless of the type of pump used in the experiment. Therefore, the presence of tight junction proteins was confirmed with both types of pumps.

4 Concluding remarks

We have developed a palmtop-sized microfluidic cell culture system driven by a miniaturized infusion pump. Both HMEC-1 and HUVEC reached confluence in the system. HMEC-1 in the system proliferated with a rate similar to that of cells cultured with a syringe pump and in a culture flask. HUVEC was oriented in the microchannel regardless of the type of pump used in the experiment. The presence of tight junction proteins between the endothelial cells was, for the first time, directly confirmed by immunostaining of Claudin-5. We expect that the palmtop-sized microfluidic cell culture system is applicable to various cell types as a stand-alone and easy-to-use system for microfluidic bioanalysis.

The authors thank Prof. R. Shimada (Department of Mathematical and Physical Sciences, Faculty of Science, Japan Women's University) for her assistance with microfabrication. This work was partially supported by the JGC Corporation and JST CREST (Core Research for Evolutional Science & Technology).

The authors have declared no conflict of interest.

5 References

[1] Lenshof, A., Laurell, T., *Chem. Soc. Rev.* 2010, *39*, 1203–1217.

[2] Wu, M.-H., Huang, S.-B., Lee, G.-B., *Lab Chip* 2010, *10*, 939–956.

[3] Yamada, M., Kano, K., Tsuda, Y., Kobayashi, J., Yamato, M., Seki, M., Okano, T., *Biomed. Microdev.* 2007, *9*, 637–645.

[4] Petersson, F., Åberg, L., Swärd-Nilsson, A.-M., Laurell, T., *Anal. Chem.* 2007, *79*, 5117–5123.

[5] Hung, P. J., Lee, P. J., Sabounchi, P., Lin, R., Lee, L. P., *Biotechnol. Bioeng.* 2005, *89*, 1–8.

[6] Young, E. W. K., Simmons, C. A., *Lab Chip* 2010, *10*, 143–160.

[7] Fidkowski, C., Kaazempur-Mofrad, M. R., Borenstein, J., Vacanti, J. P., Langer, R., Wang, Y., *Tissue Eng.* 2005, *11*, 302–309.

[8] Golden, A. P., Tien, J., *Lab Chip* 2007, *7*, 720–725.

[9] Shin, M., Matsuda, K., Ishii, O., Terai, H., Kaazempur-Mofrad, M., Borenstein, J., Detmar, M., Vacanti, J. P., *Biomed. Microdev.* 2004, *6*, 269–278.

[10] Lindström, S., Mori, K., Ohashi, T., Andersson-Svahn, H., *Electrophoresis* 2009, *30*, 4166–4171.

[11] Chrobak, K. M., Potter, D. R., Tien, J., *Microvasc. Res.* 2006, *71*, 185–196.

[12] Song, J. W., Cavnar, S. P., Walker, A. C., Luker, K. E., Gupta, M., Tung, Y.-C., Luker, G. D., Takayama, S., *PLoS ONE* 2009, *4*, e5756.

[13] Tkachenko, E., Gutierrez, E., Ginsberg, M. H., Groisman, A., *Lab Chip* 2009, *9*, 1085–1095.

[14] Chau, L., Doran, M., Cooper-White, J., *Lab Chip* 2009, *9*, 1897–1902.

[15] van der Meer, A. D., Poot, A. A., Feijen, J., Vermes, I., *Biomicrofluidics* 2010, *4*, 011103.

[16] Shao, J., Wu, L., Wu, J., Zheng, Y., Zhao, H., Jin, Q., Zhao, J., *Lab Chip* 2009, *9*, 3118–3125.

[17] Chin, L. K., Yu, J. Q., Fu, Y., Yu, T., Liu, A. Q., Luo, K. Q., *Lab Chip* 2011, *11*, 1856–1863.

[18] Song, J. W., Gu, W., Futai, N., Warner, K. A., Nor, J. E., Takayama, S., *Anal. Chem.* 2005, *77*, 3993–3999.

[19] Nalayanda, D. D., Puleo, C. M., Fulton, W. B., Wang, T. H., Abdullah, F., *Exp. Lung Res.* 2007, *33*, 321–335.

[20] Nalayanda, D. D., Wang, Q., Fulton, W. B., Wang, T.-H., Abdullah, F., *J. Pediatr. Surg.* 2010, *45*, 45–51.

[21] Esch, M. B., Post, D. J., Shuler, M. L., Stokol, T., *Tissue Eng. A* 2011, *17*, 2965–2971.

[22] Huh, D., Matthews, B. D., Mammoto, A., Montoya-Zavala, M., Hsin, H. Y., Ingber, D. E., *Science* 2010, *328*, 1662–1668.

[23] Young, E. W. K., Watson, M. W. L., Srigunapalan, S., Wheeler, A. R., Simmons, C. A., *Anal. Chem.* 2010, *82*, 808–816.

[24] Douville, N. J., Tung, Y.-C., Li, R., Wang, J. D., El-Sayed, M. E. H., Takayama, S., *Anal. Chem.* 2010, *82*, 2505–2511.

[25] Vogel, P. A., Halpin, S. T., Martin, R. S., Spence, D. M., *Anal. Chem.* 2011, *83*, 4296–4301.

[26] Leclerc, E., David, B., Griscom, L., Lepioufle, B., Fujii, T., Layrolle, P., Legallaisa, C., *Biomaterials* 2006, *27*, 586–595.

[27] Kou, S., Pan, L., van Noort, D., Meng, G., Wu, X., Sun, H., Xu, J., Lee, I., *Biochem. Biophys. Res. Commun.* 2011, *408*, 350–355.

[28] Sato, K., Mawatari, K., Kitamori, T., *Lab Chip* 2008, *8*, 1992–1998.

[29] Tanaka, Y., Kikukawa, Y., Sato, K., Sugii, Y., Kitamori, T., *Anal. Sci.* 2007, *23*, 261–266.

[30] Yamashita, T., Tanaka, Y., Idota, N., Sato, K., Mawatari, K., Kitamori, T., *Biomaterials* 2011, *32*, 2459–2465.

[31] Jang, K., Sato, K., Igawa, K., Chung, U.-I., Kitamori, T., *Anal. Bioanal. Chem.* 2008, *390*, 825–832.

[32] Herricks, T., Seydel, K. B., Turner, G., Molyneux, M., Heyderman, R., Taylor, T., Rathod, P. K., *Lab Chip* 2011, *11*, 2994–3000.

[33] Bowen, A. L., Martin, R. S., *Electrophoresis* 2010, *31*, 2534–2540.

[34] Gómez-Sjöberg, R., Leyrat, A. A., Pirone, D. M., Chen, C. S., Quake, S. R., *Anal. Chem.* 2007, *79*, 8557–8563.

[35] Futai, N., Gu, W., Song, J. W., Takayama, S., *Lab Chip* 2006, *6*, 149–154.

[36] Ades, E. W., Candal, F. J., Swerlick, R. A., George, V. G., Summers, S., Bosse, D. C., Lawley, T. J., *J. Invest. Dermatol.* 1992, *99*, 683–690.

[37] Hosokawa, K., Fujii, T., Endo, I., *Anal. Chem.* 1999, *71*, 4781–4785.

[38] Imura, Y., Asano, Y., Sato, K., Yoshimura, E., *Anal. Sci.* 2009, *25*, 1403–1407.

[39] Hosokawa, K., Sato, K., Ichikawa, N., Maeda, M., *Lab Chip* 2004, *4*, 181–185.

[40] Young, E. W., Simmons, C. A., *Lab Chip* 2010, *10*, 143–160.

[41] Morita, K., Sasaki, H., Furuse, M., Tsukita, S., *J. Cell Biol.* 1999, *147*, 185–194.

[42] Tarbell, J. M., *Cardiovasc. Res.* 2010, *87*, 320–330.

[43] Rodewald, M., Herr, D., Duncan, W. C., Fraser, H. M., Hack, G., Konrad, R., Gagsteiger, F., Kreienberg, R., Wulff, C., *Human Reprod.* 2009, *24*, 1191–1199.

[44] Beese, M., Wyss, K., Haubitz, M., Kirsch, T., *BMC Cell Biol.* 2010, *11*, 68.

JAPANESE DERMATOLOGICAL ASSOCIATION
THE JOURNAL OF DERMATOLOGY

doi: 10.1111/j.1346-8138.2011.01396.x

Journal of Dermatology 2012; **39**: 366–374

ORIGINAL ARTICLE

Targeted overexpression of Angptl6/angiopoietin-related growth factor in the skin promotes angiogenesis and lymphatic vessel enlargement in response to ultraviolet B

Hidenori OKAZAKI,[1] Satoshi HIRAKAWA,[2] Masachika SHUDOU,[3] Yoshiki NAKAOKA,[1] Yuji SHIRAKATA,[1] Keishi MIYATA,[4,5] Yuichi OIKE,[4] Koji HASHIMOTO,[1] Koji SAYAMA[1]

[1]Department of Dermatology, Ehime University Graduate School of Medicine, Ehime, [2]Department of Dermatology, Hamamatsu University School of Medicine, Shizuoka, [3]Department of Bioscience, Ehime University, Ehime, [4]Departments of Molecular Genetics, and [5]Immunology, Allergy and Vascular Medicine, Graduate School of Medical Sciences, Kumamoto University, Kumamoto, Japan

ABSTRACT

Angiogenesis is required for physiological tissue repair processes, such as cutaneous wound healing. However, recent studies indicate that endogenous angiogenic factors may enhance photo-induced skin alterations in response to experimental ultraviolet (UV)-B exposure. Angiopoietin-related growth factor (AGF), also known as angiopoietin-like protein 6 (Angptl6), is known to promote new blood vessel formation and vascular hyperpermeability. Importantly, epidermal overexpression of Angptl6/AGF in mice promotes wound healing in the skin. However, it remains unclear whether overexpression of Angptl6/AGF facilitates tissue repair processes in response to UV-B irradiation. To test this hypothesis, we subjected *Angptl6/AGF* transgenic mice to acute or chronic UV-B exposure. Surprisingly, transgenic mice showed enhanced photosensitivity to subthreshold doses of UV-B that did not induce skin alterations in wild-type littermates. Marked enlargement of blood vessels was observed after a single exposure to UV-B in *Angptl6/AGF* transgenic mice, although no epidermal changes were observed. Chronic UV-B exposure over 14 weeks promoted cutaneous skin damage in *Angptl6/AGF* transgenic mice, whereas wild-type mice showed little or no macroscopic skin alteration. In addition to pronounced angiogenesis and epidermal hyperplasia, marked enlargement of dermal lymphatic vessels was observed in UV-B-exposed *Angptl6/AGF* transgenic mice. Electron microscopy analysis further revealed that the number and size of collagen bundles in the dermis was markedly reduced after chronic UV-B exposure in *Angptl6/AGF* transgenic mice. Taken together, these results indicate that ectopic expression of Angptl6/AGF in mice likely promotes UV-B-induced skin alterations, and that angiogenesis could be a therapeutic target in prevention of skin photo-aging.

Key words: collagen, photoaging, photosensitivity, transgenic mice, vascular endothelial growth factor.

INTRODUCTION

Angiogenesis – the formation of new blood vessels from pre-existing ones – is induced in physiological tissue repair and in pathological conditions such as cutaneous inflammation and/or tumor progression.[1,2] Ultraviolet (UV)-B induces acute and chronic skin alterations. Acute exposure of human or mouse skin to UV-B promotes erythema and/or blisters because of marked increases in vascular permeability. UV-B-induced skin damage is characterized by epidermal hyperplasia, degradation of matrix proteins and dermal elastosis.[3] Previous studies have shown that pronounced angiogenesis is induced by acute UV-B irradiation of human and mouse skin.[4,5] In fact, UV-B irradiation upregulates potent angiogenic factors in the skin, including vascular endothelial growth factor (VEGF)-A, basic fibroblast growth factor and interleukin-8.[6–8] Overexpression of VEGF-A in the epidermis has also been shown to induce enhanced photosensitivity in the skin in response to a single UV-B exposure.[9] In contrast, systemic blockade of endogenous VEGF-A signaling significantly reduces photosensitivity and antagonizes enlargement of blood vessels in the skin, indicating that the primary angiogenic response may be the crucial event that facilitates acute photo-induced skin reactions. Importantly, chronic UV-B exposure caused prominent wrinkle formation in VEGF-A transgenic mice by promoting significant new blood vessel formation in the skin, leading to the idea that endogenous angiogenic factors such as VEGF-A function to promote photo-induced skin damage. Currently, it is unclear whether ectopic expression of angiogenic growth factors contributes to cutaneous tissue repair processes in response to UV-B exposure.

Angiopoietin-related growth factor (AGF), also known as Angptl6, is a member of the family of angiopoietin-like proteins, which play crucial roles in murine vascular development and/or physiological

Correspondence: Satoshi Hirakawa, M.D., Ph.D., Department of Dermatology, Hamamatsu University School of Medicine, 1-20-1 Handayama, Higashi-ku, Hamamatsu-shi, Shizuoka 431-3192, Japan. Email: hirakawa@hama-med.ac.jp
Received 17 July 2011; accepted 25 July 2011.

metabolism.[10,11] Like all angiopoietins, Angptl6/AGF possesses an N-terminal coiled-coil domain and a C-terminal fibrinogen-like domain.[12] Most angiopoietins are known to bind Tie1 and/or Tie2 receptors, whereas Angptl6/AGF remains an orphan ligand. Targeted disruption of *Angptl6/AGF* in mice leads to obesity and insulin resistance, reflecting clinical features reminiscent of human metabolic syndrome.[11] Meanwhile, targeted overexpression of Angptl6/AGF in mouse skin promotes angiogenesis and epidermal hyperplasia, indicating that Angptl6/AGF mediates pleiotropic effects towards several cell lineages, including epidermal keratinocytes.[10,13] Of particular interest, Angptl6/AGF transgenic mice in the skin show markedly enhanced cutaneous wound healing during the tissue repair process compared to wild-type mice.[13] Importantly, little or no Angptl6/AGF is expressed endogenously in mouse skin, indicating that Angptl6/AGF has a potent tissue repair function separate from its role as an angiogenic factor in the skin.

Recent studies indicate that lymphatic vessels play a crucial role in mediating UV-B-induced cutaneous changes.[14] UV-B exposure induces marked enlargement of lymphatic vessels in mouse skin. Sufficient lymphatic flow is required to suppress dermal edema and inflammation in response to a single UV-B exposure. Importantly, activation of VEGF-C/vascular endothelial growth factor receptor-3, one of the major pathways promoting lymphatic vessel growth and function,[15] has been shown to attenuate UV-B-induced edema formation and skin inflammation.[16] Furthermore, lymphatic vessels show enhanced leakiness in UV-B-irradiated skin, leading to reduced lymphatic drainage and impaired function.[14] Moreover, among Angptl family members, targeted Angptl2 overexpression in the skin has been recently shown to promote enlargement of dermal lymphatic as well as blood vessels.[17] Currently, it is unclear whether Angptl6/AGF alters the growth of lymphatic vessels in experimental mouse models of UV-B exposure.

Here, to test the hypothesis whether AGF facilitates cutaneous tissue repair processes in response to UV-B irradiation, we subjected *Angptl6/AGF* transgenic mice to either acute or chronic UV-B exposure. We report that overexpression of Angptl6/AGF in mouse skin enhances photosensitivity to acute UV-B exposure by promoting enlargement of dermal blood vessels but does not induce epidermal hyperplasia in response to a minimal erythema dose of UV-B. By contrast, chronic UV-B exposure, at a dose that did not induce detectable skin changes in wild-type mice, induced pronounced angiogenesis and enlargement of lymphatic vessels, leading to wrinkle development in *Angptl6/AGF* transgenic mice. Together, these results indicate that targeted overexpression of Angptl6/AGF in mouse skin may prevent photo-induced cutaneous damage from a single exposure of UV-B, but long-term AGF induction could mediate UV-B-induced skin alterations such as photo-induced skin aging.

METHODS

UV-B irradiation regime

Ten-week-old male FVB/N or BALB/c wild-type mice, or keratin 14 promoter-driven *Angptl6/AGF* transgenic mice were exposed to graded doses of four equally charged fluorescent lamps (ULTRAVIOLET-B TL 20W/12RS; Philips, Amsterdam, Netherlands). The minimal erythema dose (MED) was determined by irradiation of square areas on back skin with seven different doses of UV-B, ranging 5.0×10^{-2} to 4.0×10^{-1} J/cm^2 (n = 5/group). An additional skin area was sham-irradiated. Erythema formation was evaluated 48 h after irradiation. Ten-week-old male BALB/c wild-type mice or transgenic overexpressing Angptl6/AGF in the epidermis under control of the human keratin 14 promoter were exposed to seven different UV-B doses, ranging 3.0×10^{-2} to 9.0×10^{-2} J/cm^2, on the dorsal skin (n = 5/group) to determine MED. In addition, ear skin of AGF transgenic mice and wild-type littermates was exposed to a single dose of UV-B by 9.0×10^{-2} J/cm^2 (n = 5/group). Thereafter, ear thickness was measured daily for up to 8 days. In an additional experiment, 8-week-old male wild-type or AGF transgenic mice were irradiated three times weekly for 14 weeks with a total dose of 8.185 J/cm^2 (n = 10/genotype). Control mice were sham-irradiated. Skin samples were either snap-frozen with O.C.T.-Compound (Sakura Finetek Japan, Tokyo, Japan) in ethanol dry ice or fixed in 4% paraformaldehyde in phosphate-buffered saline. All animal studies were approved by the Ehime University Subcommittee on Research Animal Care.

Real-time reverse transcription polymerase chain reaction (RT–PCR)

Total RNA was isolated from dorsal skin of *Angptl6/AGF* transgenic mice or wild-type littermates (n = 5) and of five non-irradiated control mice using Isogen (Wako, Osaka, Japan). Real-time RT–PCR was performed and analyzed with a 7900 HT Fast Real-Time PCR System (Applied Biosystems, Branchburg, NJ, USA). Primers and probes for β-actin, AGF, VEGF-A, VEGF-C and VEGF-D were purchased from Applied Biosystems. RNA analysis was carried out using a TaqMan RT–PCR Master Mix reagents kit (Applied Biosystems), according to the manufacturer's protocol. Target gene expression in test samples was normalized to corresponding β-actin expression.

Histological analysis and immunofluorescence stains

Immunofluorescence was analyzed on 5-μm frozen sections, as described previously,[18] using a biotinylated rat antimouse CD31 antibody (BD Biosciences Pharmingen, San Diego, CA, USA), a monoclonal rat LYVE-1 antibody (MBL, Nagoya, Japan), and corresponding secondary antibodies labeled with Alexa Fluor 488 or 594 (Molecular Probes, Eugene, OR, USA). Representative sections were prepared from skin of UV-B- or sham-irradiated mice (n = 5/group). Nuclei were counterstained with 4′,6′-diamidino-2-phenylindole dihydrochloride (DAPI; Molecular Probes). Staining was analyzed and digital images were captured using a confocal laser scanning microscope LSM510 (Carl Zeiss, Jena, Germany). Morphometric analyses were performed using IP-LAB software as described previously.[19] In addition, paraffin sections were prepared from skin of the same mice. Routine hematoxylin–eosin or Masson-trichrome staining was performed.

Computer-assisted morphometric vessel analysis

Double immunofluorescence staining using anti-CD31 antibody for blood vessels and anti-LYVE-1 antibody for lymphatic vessels was analyzed using an LSM510 microscope. Representative fields of

each section were examined at ×10 magnification, and the number of vessels/mm^2, average vessel size and relative area occupied by blood or lymphatic vessels were determined in a dermal area within 200 μm of the epidermal–dermal junction. An unpaired Student's *t*-test was used to analyze differences in microvessel density, vascular size and relative vascular area.

Transmission electron microscopy analysis

Skin tissues were fixed in 0.1 mol/L phosphate-buffered 2.5% glutaraldehyde with 0.1% tannic acid (pH 7.4) for 2 h, and postfixed with 1% osmium tetroxide in phosphate buffer for 2 h. Specimens were washed in 0.25 mol/L sucrose solution, dehydrated in a graded ethanol series, and embedded in an Epon resin mixture (Epon 812 resin; TAAB Laboratories Equipment, Aldermaston, Berks, England). Ultra-thin sections of 60–80 nm were prepared using an Ultracut S blade (Leica Microsystems, Wetzlar, Germany) and subsequently double-stained with uranyl acetate and lead citrate. Specimens were analyzed at a voltage of 80 kV, and images were captured using a transmission electron microscope, JEM-1230 (JEOL, Tokyo, Japan).

RESULTS

BALB/c and FVB/N wild-type mice show comparable MED

Transgenic mice in which Angptl6/AGF is driven from the keratin 14 promoter (*K14–Angptl6/AGF*) were originally bred on a BALB/c background.[13] However, previous studies of the role of angiogenesis in mediating UV-B-induced skin alterations in transgenic mice have utilized mice on an FVB/N background.[4,9] Therefore, to assess the biological effect of Angptl6/AGF upon photodamaged skin, we first compared the MED of wild-type FVB/N and BALB/c mice using graded UV-B doses. The dorsal skin of FVB/N wild-type mice showed signs of erythema 48 h after irradiation with 7.2×10^{-2} J/cm^2 UV-B or higher doses ($n = 6$) (Fig. 1a). Similarly, BALB/c wild-type mice developed minimal erythema on back skin at a dose of 7.2×10^{-2} J/cm^2 UV-B ($n = 6$) (Fig. 1b) in the same timeframe. Therefore, both FVB/N and BALB/c wild-type mice showed comparable erythema formation at the same radiation dose, indicating that BALB/c mice are suitable models to evaluate photosensitivity following UV-B radiation.

Cutaneous photosensitivity is enhanced in *Angptl6/AGF* transgenic mice

To determine whether epidermal Angptl6/AGF overexpression alters cutaneous photosensitivity in the skin, we evaluated MED of *Angptl6/AGF* transgenic mice by exposing them to doses of UV-B ranging 3.0×10^{-2} to 9.0×10^{-2} J/cm^2. The dorsal skin of AGF transgenic mice showed signs of erythema at 4.0×10^{-2} J/cm^2 UV-B and higher ($n = 5$) (Fig. 1d), whereas in comparably-treated wild-type littermates the MED was defined as 7.2×10^{-2} J/cm^2 UV-B (Fig. 1c). Statistical analysis showed that the MED for *Angptl6/AGF* transgenic mice is significantly lower than that of wild-type mice (Fig. 1e). Overall, these observations suggest that Angptl6/AGF transgenic mice show enhanced cutaneous photosensitivity relative to wild-type mice.

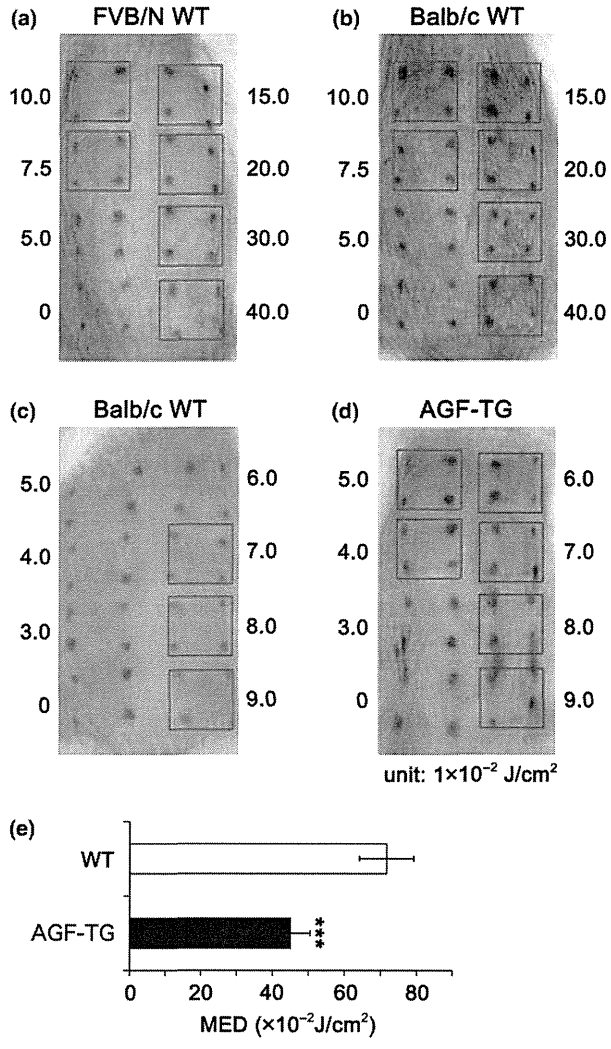

Figure 1. Enhanced photosensitivity of *Angptl6/AGF* transgenic (TG) mice. (a,b) The dorsal skin was exposed to graded doses of ultraviolet (UV)-B ranging 5.0×10^{-2} to 4×10^{-1} J/cm^2, or to sham irradiation. A minimal erythema dose (MED) of 7.5×10^{-2} J/cm^2 was determined by analyzing skin of wild-type (WT) FVB/N mice 48 h after irradiation (a, $n = 5$). A comparable MED was observed in wild-type BALB/c mice (b, $n = 5$). (c,d) Analysis of the skin of *Angptl6/AGF* transgenic mice indicated a MED of 4.0×10^{-2} J/cm^2 of UV-B (d, $n = 5$), whereas skin of wild-type littermates showed signs of erythema at 7.0×10^{-2} J/cm^2. (e, $n = 5$) Statistical analysis confirmed that the MED for *Angptl6/AGF* transgenic mice is significantly lower than that of wild-type mice. Data are expressed as mean ± standard deviation ($n = 6$/condition). ***$P < 0.001$.

Angptl6/AGF promotes blood vessel enlargement in response to a single UV-B exposure

One MED induces formation of an erythema characterized by microvascular enlargement in the skin. Therefore, we asked whether macroscopic vascular enlargement occurs in the skin of *Angptl6/AGF* transgenic mice by irradiating them with increased doses of UV-B. A dose of 9.0×10^{-2} J/cm^2 UV-B induced macroscopic

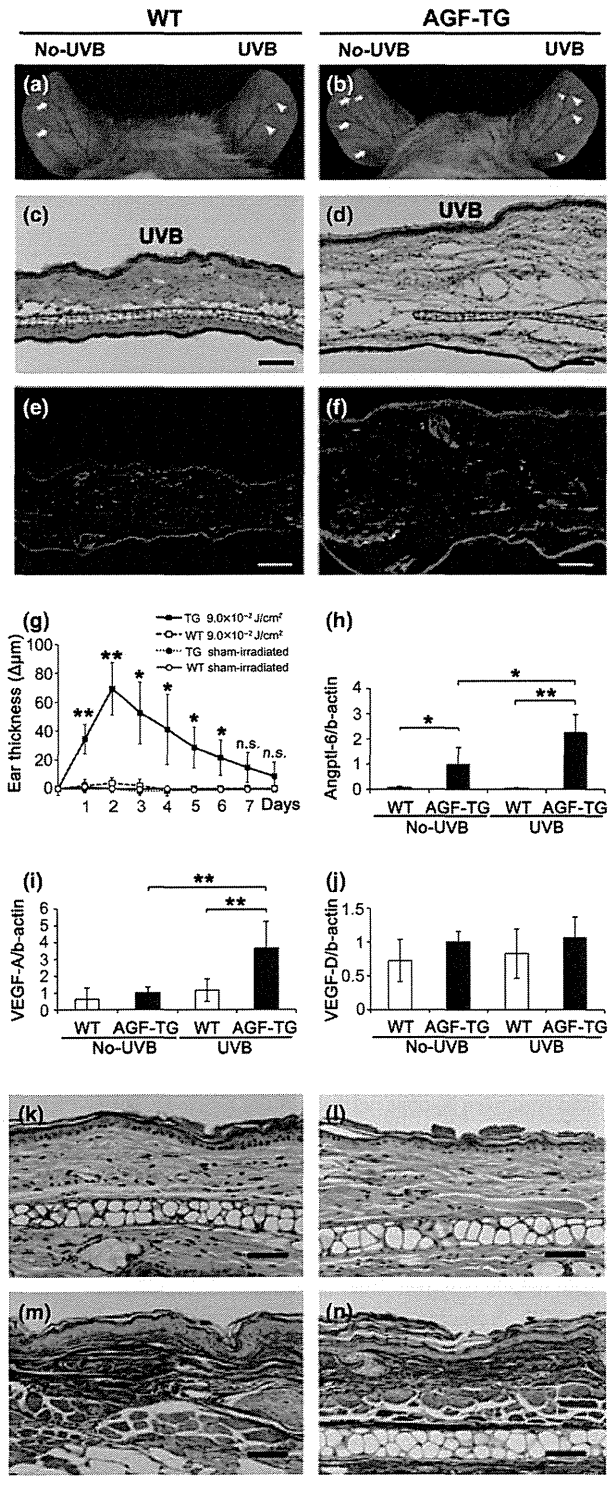

Figure 2. Angptl6/AGF promotes blood vessel enlargement following acute ultraviolet (UV)-B irradiation (a,b). The ear skin of *Angptl6/AGF* transgenic (TG) mice or wild-type (WT) littermates was exposed to a single irradiation of UV-B of 9.0×10^{-2} J/cm^2. Forty-eight hours later, transgenic mice developed erythema and enlargement of blood vessels (b, arrowheads) relative to sham-irradiated ears (b, arrows), whereas little or no alteration was observed in UV-B-exposed (a, arrowheads) or sham-irradiated ear skin of wild-type mice (a, arrows). (c,d) Histological analysis revealed that ear skin of wild-type mice appeared normal (c, hematoxylin–eosin [HE]), whereas the skin of Angptl6/AGF-overexpressing mice showed dermal edema and vessel dilation particularly on the side of UV-B irradiation as compared with the other side of ear skin which is unexposed to UV-B (d, HE). (e,f) Double immunofluorescence staining reveals dilated CD31$^+$ blood vessels (red) in transgenic mice, while no such changes were seen in skin of wild-type littermates. LYVE-1$^+$ stain (green) was comparable between ear skin of AGF transgenic mice and wild-type littermates. Nuclei are stained blue (4′,6′-diamidino-2-phenylindole dihydrochloride [DAPI] stain). (Scale bars, 100 μm.) (g) Angptl6/AGF-overexpressing mice show significant ear swelling 48 h after irradiation with 9.0×10^{-2} J/cm^2 UV-B (♦), while no ear swelling is observed in similarly treated wild-type littermates (■). (h–j) Quantitative reverse transcription polymerase chain reaction (RT–PCR) analyses of ear skin of Angptl6/AGF-overexpressing mice and wild-type littermates 48 h after UV-B irradiation (n = 5). Increased Angptl6/AGF and vascular endothelial growth factor (VEGF)-A expression was seen in K14–*Angptl6/AGF* mice in response to a single UV-B exposure (h,i). Comparable levels of VEGF-D mRNA were seen in the presence or absence of UV-B irradiation (j). Routine HE stain showed that ear skin of Angptl6/AGF-overexpressing mice and wild-type mice appeared comparable and normal 8 days after UV-B irradiation (k,l). Azan–Mallory staining showed that collagen bundles in the papillary dermis remained normal in UV-B-treated *Angptl6/AGF* transgenic mice (n) and wild-type littermates 8 days after UV-B irradiation (m). Data are expressed as means ± standard deviation (n = 5/condition and time point). $^{**}P < 0.01$; $^{*}P < 0.05$.

vascular enlargement in ear skin of *Angptl6/AGF* transgenic mice (Fig. 2b, arrowheads) as compared with sham-irradiated ears (Fig. 2b, arrows), whereas no macroscopic vascular alteration was seen in UV-B-exposed (Fig. 2a, arrowheads) or sham-irradiated ear skin of wild-type littermates (Fig. 2a, arrows). Histologically, ear skin of *Angptl6/AGF* transgenic mice showed marked edema in the dermis and vessel dilation 48 h after irradiation (Fig. 2d), whereas the skin of wild-type mice showed no significant changes at 9.0×10^{-2} J/cm^2 UV-B (Fig. 2c). Double immunofluorescence with antibodies against CD31 for blood vessels and LYVE-1 for lymphatic vessels showed that blood vessels were markedly enlarged in *Angptl6/AGF* transgenic mice (Fig. 2f), whereas no such changes were seen in wild-type littermates (Fig. 2e). Lymphatic vessels in *Angptl6/AGF* transgenic mice remained normal as well as lymphatic vessels in wild-type littermates. Furthermore, *Angptl6/AGF* transgenic mice showed prominent, albeit transient, ear swelling 48 h after irradiation (Fig. 2g). In contrast, the ears of wild-type mice showed no detectable changes in thickness after a single UV-B irradiation at 9.0×10^{-2} J/cm^2 (Fig. 2g).

Quantitative real-time RT–PCR analyses of RNA extracted from mouse ears showed that expression levels of Angptl6/AGF and VEGF-A increased by 2.0-fold (Fig. 2h) and 2.5-fold (Fig. 2i), respectively, in *Angptl6/AGF* transgenic mice 48 h after irradiation. By contrast, wild-type mice showed little or no change in expression levels of either transcript after irradiation with 9.0×10^{-2} J/cm^2

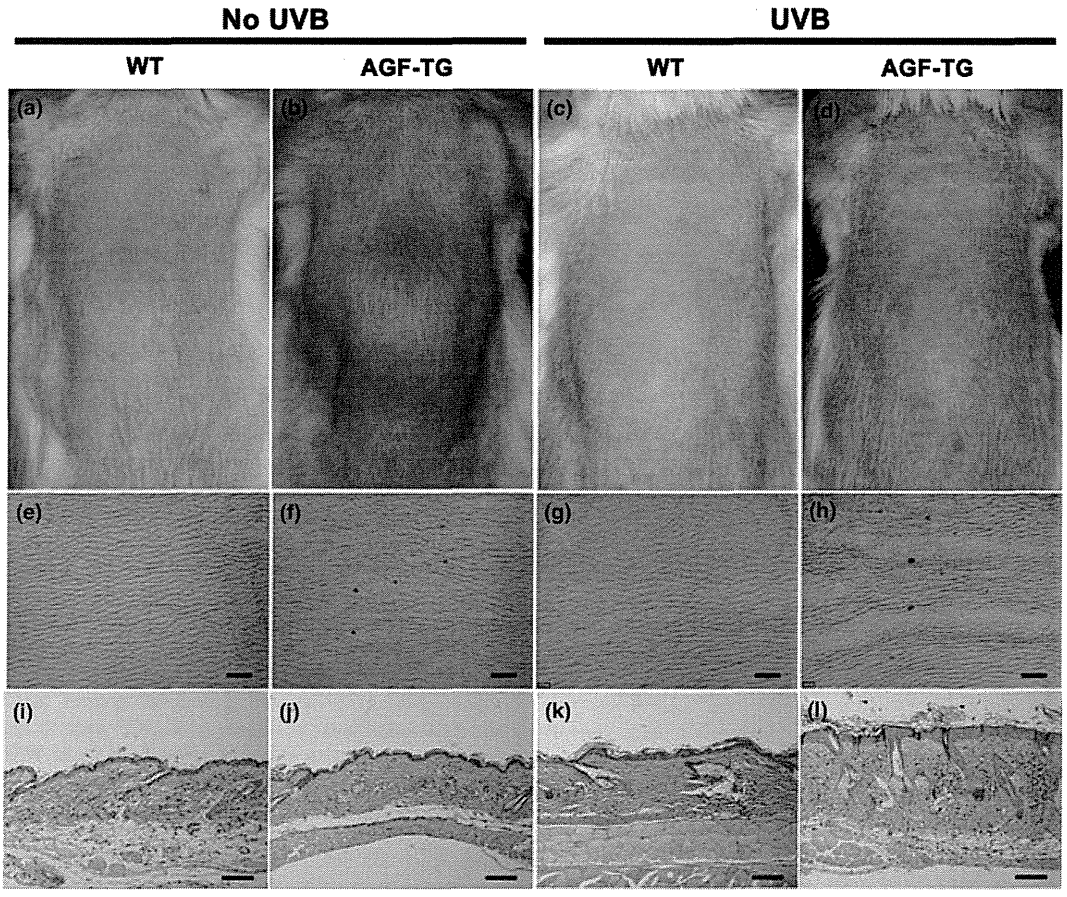

Figure 3. Increased wrinkle formation in Angptl6/AGF-overexpressing mice after long-term ultraviolet (UV)-B irradiation. Dorsal skin of non-irradiated wild-type (WT) and *Angptl6/AGF* transgenic (TG) mice (a,b). After 14 weeks (three times/week) of UV-B irradiation, wild-type mice do not show macroscopic skin alterations (c), whereas *Angptl6/AGF* transgenic mice developed wrinkles and slight erythema (d) (representative images; n = 13/genotype). Skin replicas of wild-type and Angptl6/AGF-overexpressing mice showed no signs of wrinkle formation or texture changes (e,f), nor did those of wild-type mice treated with UV-B (g). Angptl6/AGF-overexpressing mice treated with long-term UV-B irradiation, however, did show wrinkle formation and texture changes (h). (i–l) Hematoxylin–eosin (HE) staining reveals signs of epidermal hyperplasia, edema, inflammatory cell infiltration, and increased vascularization in the papillary dermis in skin of UV-B-irradiated Angptl6/AGF-overexpressing mice (l). The skin of non-irradiated mice of both genotypes (i,j), or of UV-B-irradiated wild-type mice (k) does not show major histological abnormalities. (Scale bars: [e–h] 1 mm, [i–l] 100 μm.)

UV-B. Furthermore, comparable expression levels of VEGF-D were observed in the ears of *Angptl6/AGF* transgenic and wild-type mice under UV-B- or sham-irradiation regimes (Fig. 2j). VEGF-C mRNA levels remained unchanged in either group (data not shown).

To find overall changes of ears in *Angptl6/AGF* transgenic mice and wild-type littermates, we daily measured the ear thickness for 8 days after UV-B irradiation. Seven days after UV-B irradiation, ear thickness was comparable between AGF transgenic mice and wild-type littermates (Fig. 2g). Eight days after UV-B irradiation, the macroscopic appearance of ear skin in *Angptl6/AGF* transgenic mice returned to normal (data not shown). Histologically, ears obtained from *Angptl6/AGF* transgenic mice and wild-type littermates showed comparable cellular morphology 8 days after irradiation based on hematoxylin–eosin staining (Fig. 2k,l). Azan–Mallory staining also indicated little or no degradation of dermal collagen bundles in ears of *Angptl6/AGF* transgenic mice 8 days after irradiation with 9.0×10^{-2} J/cm^2 UV-B (Fig. 2m,n). Together, these results suggest that targeted overexpression of Angptl6/AGF promotes vascular enlargement and subsequent plasma leakage from blood vessels at early stages of UV-B irradiation in murine skin, but that vascular hyperpermeability is not associated with acute photo-induced skin damage.

Angptl6/AGF mediates epidermal hyperplasia in response to chronic UV-B exposure

Overall, we found transient vascular enlargement and reversible ear swelling in *Angptl6/AGF* transgenic mice after a single UV-B exposure but did not observe acute UV-B-induced skin damage or acceleration of the healing process. Therefore, we asked whether targeted Angptl6/AGF overexpression induces skin changes

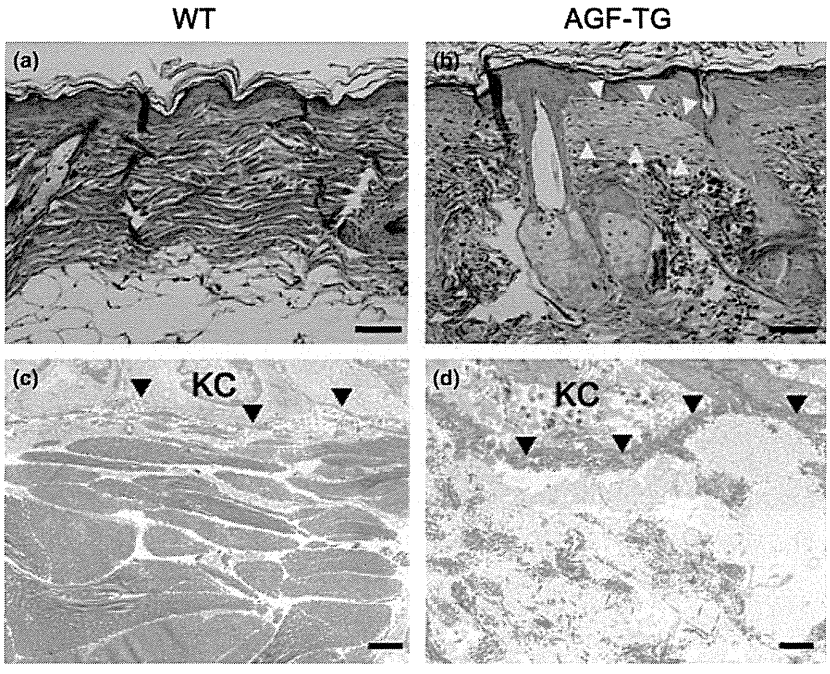

Figure 4. Marked reduction in dermal collagen bundles in *K14–Angptl6/AGF* transgenic mice after long-term ultraviolet (UV)-B. (a,b) Azan–Mallory staining shows that collagen bundles in the papillary dermis are severely altered in UV-B-treated *Angptl6/AGF* transgenic (TG) mice (b, yellows arrows) compared with wild-type (WT) littermates (a). (c,d) Electron micrographs revealed that collagen fibrils and bundles in UV-B-treated AGF transgenic mice were markedly fragmented beneath the dermoepidermal junction (d, arrowheads) compared with wild-type mice (c, arrowheads). (Scale bars: [a,b] 50 μm, [c,d] 2 μm.) KC, keratinocytes.

following chronic UV-B irradiation. *Angptl6/AGF* transgenic mice and wild-type littermates were exposed 3 days a week to a total dose of 8.185 J/cm^2 UV-B for 14 weeks. Wild-type mice showed no skin changes after UV-B irradiation based on both macroscopic appearance (Fig. 3c) and microscopic analysis using skin replicas (Fig. 3g) and appeared comparable in gross appearance to sham-irradiated wild-type mice (Fig. 3a,e). In contrast, the skin of *Angptl6/AGF* transgenic mice exhibited transverse wrinkles after chronic UV-B irradiation (Fig. 3d,h), while sham-irradiated transgenic mice showed little or no wrinkling (Fig. 3b,f). Histologically, the skin of *Angptl6/AGF* transgenic mice showed evidence of epidermal hyperplasia, edema formation and inflammatory cell infiltration in the dermis after chronic UV-B irradiation (Fig. 3l), whereas no such changes were observed in sham-irradiated transgenic mice (Fig. 3j) or in wild-type mice with or without UV-B irradiation (Fig. 3i,k). Azan–Mallory staining showed that the size of collagen bundles was reduced in the upper dermis of *Angptl6/AGF* transgenic mice after chronic UV-B exposure (Fig. 4b), whereas these alterations were not observed in UV-B-irradiated wild-type littermates (Fig. 4a). Moreover, electron microscopic analysis revealed that the regular assembly of collagen was markedly perturbed in the upper dermis of *Angptl6/AGF* transgenic mice after chronic UV-B irradiation (Fig. 4d), whereas the fibrillar collagen network was maintained in the dermis of UV-B-irradiated wild-type mice (Fig. 4c). Together, these results suggest that following chronic UV-B exposure, the skin of *Angptl6/AGF* transgenic mice undergoes alterations leading to wrinkle formation.

Targeted Angptl6/AGF overexpression promotes angiogenesis and lymphatic enlargement in response to chronic UV-B exposure

To determine whether chronic UV-B exposure alters the microvascular network in the skin of *Angptl6/AGF* transgenic mice, we undertook macroscopic and microscopic analyses of blood and lymphatic vessels in the skin. Macroscopic analysis indicated that the skin of transgenic mice was more vascularized after UV-B exposure than that of wild-type littermates either with or without irradiation (Fig. 5a,c,d) or of sham-irradiated transgenic mice (Fig. 5b). Double staining for blood and lymphatic vessels showed that CD31-positive blood vessels were enlarged in the upper dermis of *Angptl6/AGF* transgenic mice after chronic UV-B irradiation (Fig. 5h), whereas few alterations were seen in sham-irradiated transgenic mice or wild-type littermates, either irradiated or not irradiated (Fig. 5e–g). Computer-assisted morphometric analysis of CD31-stained skin sections confirmed that the average number of blood vessels was significantly increased in *Angptl6/AGF* transgenic mice after chronic irradiation (47.23 ± 8.65 blood vessels/mm^2; $P < 0.05$), as compared with sham-irradiated transgenic mice (32.17 ± 3.25 blood vessels/mm^2) or wild-type controls (25.45 ± 3.36 blood vessels/mm^2; Fig. 5j). Furthermore, blood vessels were significantly larger in UV-B-irradiated *Angptl6/AGF* transgenic mice (353.6 ± 41.7 μm^2; $P < 0.05$) than in sham-irradiated transgenic mice (295.6 ± 35.3 μm^2; Fig. 5k). Moreover, we observed a significant increase in the percentage of total tissue area covered by blood vessels in UV-B-irradiated *Angptl6/AGF*

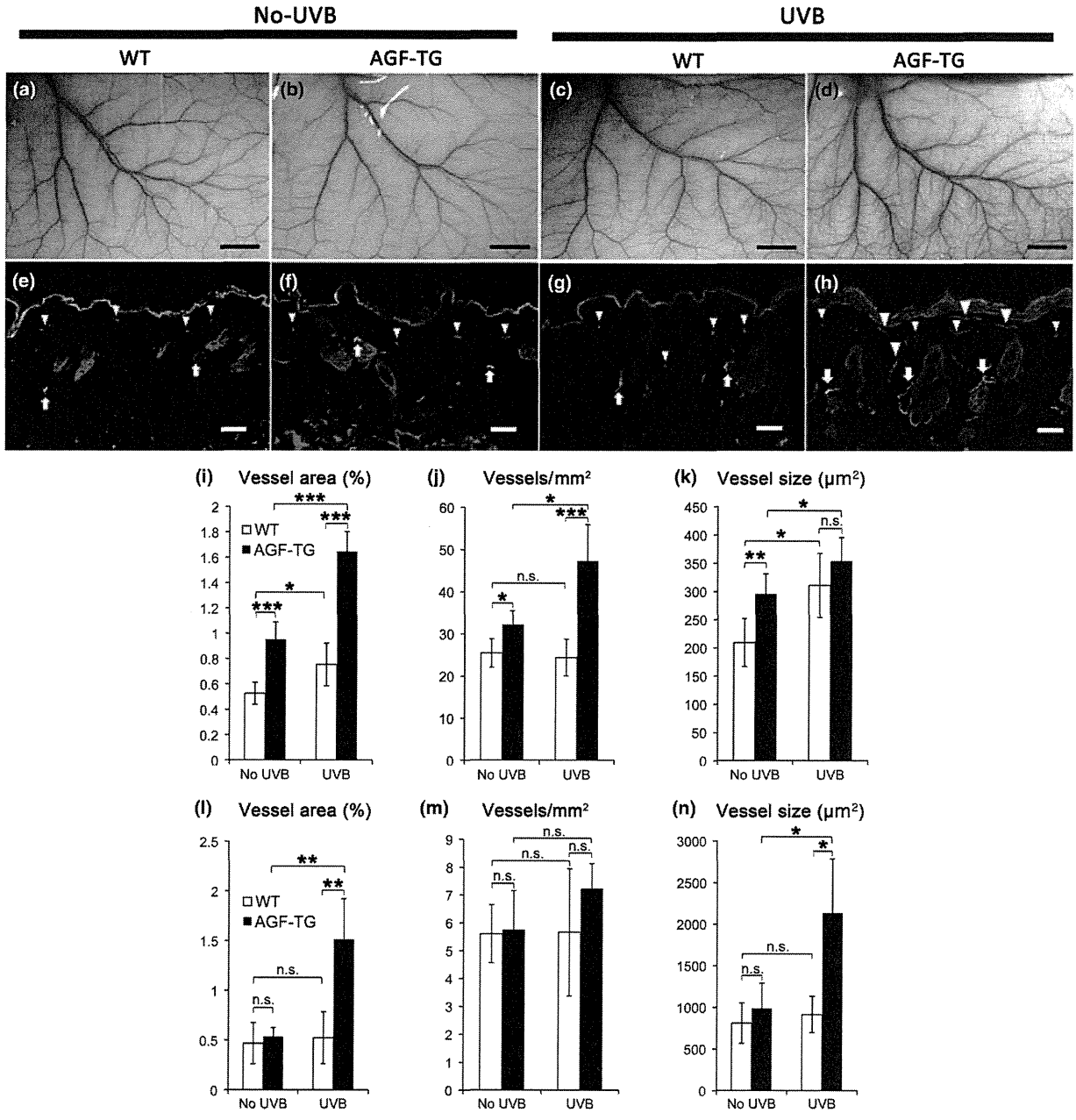

Figure 5. Induction of angiogenesis in *Angptl6/AGF* transgenic (TG) mice after long-term ultraviolet (UV)-B irradiation. (a–d) Increased cutaneous vascularization, with prominent enlargement of blood vessels, is observed after chronic UV-B treatment in the skin of Angptl6/AGF-overexpressing mice (d). Compared with non-irradiated wild-type (WT) littermates (a), no significant changes were observed in wild-type littermates after long-term UV-B irradiation (c) or in Angptl6/AGF-overexpressing mice that did not undergo irradiation (b). (Scale bars: 3 mm.) (e–h) Double immunofluorescence for blood vessels by anti-CD31 antibody (red, arrowheads) and for lymphatic vessels by anti-LYVE-1 antibody (green, arrows) demonstrates prominent vascularization in the dermis of Angptl6/AGF-overexpressing mice after chronic UV-B irradiation (h), whereas few vessels were altered in wild-type littermates that did or did not undergo UV-B irradiation (e,g) and in non-irradiated Angptl6/AGF-overexpressing mice (f). (Scale bars, 50 μm.) (i) Computer-assisted morphometric analysis of CD31-stained skin sections after 14 weeks of UV-B irradiation revealed a significant increase in the relative area occupied by blood vessels (i) and in blood vessel density (j) in *Angptl6/AGF* transgenic mice (■) compared with wild-type littermates (□). (k) Enlargement of blood vessels detected by CD31 staining is prominent in UV-B-treated *Angptl6/AGF* transgenic mice. Skin sections after 14 weeks of UV-B irradiation show a significant increase in the relative area occupied by lymphatic vessels (l) and in average vessel size (n) in *Angptl6/AGF* transgenic mice (■) compared with wild-type mice. In contrast, no significant differences were observed in the vessel density (m) between non-irradiated and irradiated skin of AGF transgenic mice (■) and wild-type littermates (□). Data are expressed as mean ± standard deviation ($n = 5$). ***$P < 0.001$; **$P < 0.01$; *$P < 0.05$.

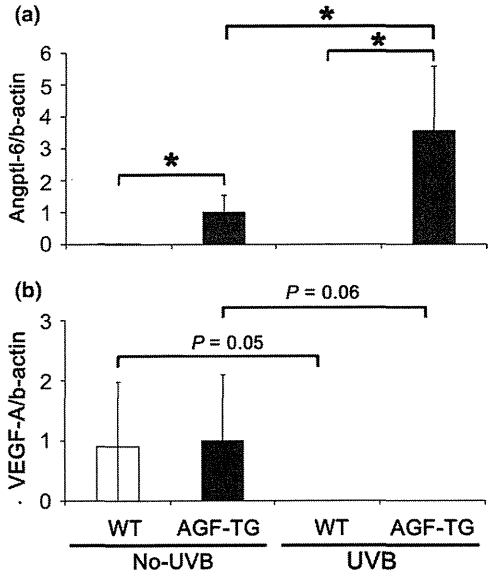

Figure 6. Chronic ultraviolet (UV)-B exposure promotes increased levels of Angptl6/AGF mRNA and decreased levels of vascular endothelial growth factor (VEGF)-A mRNA. (a) Angptl6/AGF mRNA levels were significantly increased in the skin of UV-B-exposed transgenic (TG) mice compared with wild-type littermates. (b) In contrast, VEGF-A mRNA expression in the skin was undetectable after UV-B irradiation of either wild-type or *Angptl6/AGF* transgenic mice.

transgenic mice (1.65 ± 0.16%) compared with controls (0.75 ± 0.17%; $P < 0.001$) (Fig. 5i). Lymphatic-specific staining with LYVE-1 revealed marked enlargement of dermal lymphatic vessels in UV-B-irradiated skin of *Angptl6/AGF* transgenic mice (Fig. 5h) compared with sham-irradiated transgenic mice (Fig. 5f) or irradiated or non-irradiated wild-type mice (Fig. 5e,g). Computer-assisted morphometric analysis showed that the size of dermal lymphatic vessels is significantly increased by twofold ($P < 0.05$) in *Angptl6/AGF* transgenic mice after chronic UV-B irradiation (2129.2 ± 654.1 μm^2; $P < 0.05$) compared with non-irradiated transgenic mice (981.5 ± 305.4 μm^2), or wild-type controls with or without UV-B irradiation (911.2 ± 219.3 μm^2 or 807.7 ± 242.6 μm^2, respectively; Fig. 5n). The percentage of total tissue area covered by lymphatic vessels of *Angptl6/AGF*-overexpressing skin was significantly increased after chronic UV-B-irradiation (1.51 ± 0.41%; $P < 0.001$) compared with sham-irradiated *Angptl6/AGF* transgenic mice (0.53 ± 0.09%) or wild-type controls with or without UV-B irradiation (0.52 ± 0.26% or 0.47 ± 0.21%, respectively; Fig. 5l). However, the average density of dermal lymphatics in both genotypes with or without chronic UV-B exposure was comparable (Fig. 5m). Importantly, increased levels of ectopic *Angptl6/AGF* mRNA were observed in UV-B-exposed skin of *Angptl6/AGF* transgenic mice as compared with sham-irradiated skin of transgenic mice (Fig. 6). No changes in VEGF-A mRNA levels were observed in UV-B-exposed skin of either *Angptl6/AGF* transgenic or wild-type mice (Fig. 6). Together, these results suggest that overexpression of *Angptl6/AGF* in mouse skin promotes prominent angiogenesis and subsequent enlargement of lymphatic vessels.

DISCUSSION

In this study, we subjected *Angptl6/AGF* transgenic mice to UV-B exposure, a major risk for cutaneous damage, to test the hypothesis that Angptl6/AGF might reduce acute and/or chronic skin damage by accelerating tissue repair. Interestingly, however, our results indicate that chronic UV-B activates the K14 promoter driving the Angptl6/AGF transgene, resulting in photo-induced skin alterations at a subthreshold UV-B dose that induced little or no skin changes in wild-type littermates.

Recent studies indicate that UV-B potently induces an angiogenic switch, namely, upregulates pro-angiogenic mediators and downregulates anti-angiogenic ones, leading to a pathological pro-angiogenic condition in the skin.[9] In support of this concept, targeted VEGF-A overexpression in mouse skin was shown to promote vascular enlargement and subsequent vascular leakage in response to a single UV-B exposure.[9] In addition, VEGF-A transgenic mice showed increased inflammatory cell infiltration in the dermis and epidermal hyperplasia at subthreshold UV-B doses, features typical of acute UV-B-induced skin damage.[9] In contrast, in the present study, targeted Angptl6/AGF overexpression in mouse skin promoted little or no epidermal hyperplasia in response to a single UV-B exposure, although marked enlargement of cutaneous blood vessels was observed. In fact, Angptl6/AGF has been shown to increase the vascular network of capillary-sized blood vessels in a physiological pattern,[17] whereas VEGF-A induces formation of tortuous, capillary-sized blood vessels in transgenic mice, leading to promotion of leukocyte trafficking and rolling.[20] Therefore, physiological induction of AGF by a single UV-B exposure may prevent enhanced vascular leakage, which would initiate cutaneous inflammation and subsequent epidermal hyperplasia.

In contrast to a single UV-B exposure, chronic UV-B exposure over 14 weeks was accompanied by prominent skin alterations, including epidermal hyperplasia, in *Angptl6/AGF* transgenic mice as compared with wild-type littermates. Overproduction of AGF over a long period may underlie the development of wrinkles seen in response to chronic UV-B irradiation. In fact, in this study, a total dose of 8.156 J/cm^2 UV-B was required to promote development of macroscopic wrinkles in *K14–Angptl6/AGF* transgenic mice, whereas a total dose of 0.72 J/cm^2 UV-B was sufficient to induce chronic photo-induced skin damage in irradiated *K14–VEGF-A* transgenic mice.[9] Interestingly, no induction of VEGF-A mRNA was found in *Angptl6/AGF* transgenic mice which were exposed to the long-term UV-B irradiation in the skin, whereas *Angptl6/AGF* mRNA levels were significantly increased in those mice. Therefore, these findings suggest that long-term UV-B irradiation activates the K14 promoter driving the *Angptl6/AGF* transgene, and that the ectopic overexpression of AGF actively promotes the development of chronic photo-induced skin alterations in an independent manner.

Dermal lymphatic vessels were markedly enlarged in *Angptl6/AGF* transgenic mice after chronic UV-B exposure. In contrast, little or no lymphatic vessel alteration was seen in sham-irradiated *Angptl6/AGF* transgenic mice compared with wild-type littermates. Does experimental induction of Angptl6/AGF by chronic UV-B exposure mediate dilation of lymphatic vessels? The skin of

UV-B-exposed *Angptl6/AGF* transgenic mice exhibits signs of enhanced angiogenesis reflected by an increased number of blood vessels compared to sham-irradiated mice. In contrast, the density of lymphatic vessels was comparable between chronic UV-B- and sham-irradiated *Angptl6/AGF* mice, suggesting that Angptl6/AGF does not induce lymphangiogenesis as it does angiogenesis. However, increased blood flow can induce uptake and subsequent transport of fluids by dermal lymphatic vessels, likely promoting significant enlargement of the lymphatic vasculature. Importantly, chronic UV-B exposure markedly upregulated Angptl6/AGF mRNA levels, whereas no upregulation of VEGF-A mRNA levels was observed in this model. VEGF-A, but not VEGF-C or VEGF-D, was previously shown to be upregulated in *hairless* mice in response to chronic UV-B exposure, an effect accompanied by enlargement and impairment of lymphatic vessels.[14] Furthermore, functional inactivation of VEGF-A inhibits enlargement of lymphatic vessels after a single UV-B exposure, suggesting that VEGF-A is responsible for both vascular hyperpermeability and reduced lymphatic drainage in response to UV-B exposure.[14] Therefore, angiogenesis and increased blood flow likely promote enlargement of lymphatic vessels and alter their function in chronic UV-B-induced skin damage. Accordingly, Angptl6/AGF has been recently shown to enhance blood flow in a mouse hind-limb ischemia model.[21] In addition, epidermal overexpression of Angptl2 promotes marked enlargement of lymphatic and blood vessels in the skin. Moreover, sufficient lymphatic flow is required to minimize tissue edema and subsequent inflammation in response to UV-B irradiation.[22] Therefore, future studies should address whether UV-B irradiation alters lymphatic flow and/or function in Angptl transgenic mice, and whether metastasis associated with UV-B-induced carcinogenesis is correlated with changes in lymphatic vessel function.

ACKNOWLEDGMENTS

The authors thank Mika Ikeda, Eriko Tan and Teruko Tsuda for technical assistance. The Japanese Society for Investigative Dermatology Fellowship SHISEIDO Award 2008 (to S. H.), and a Grant-in-Aid for Scientific Research from the Ministry of Education, Culture, Sports, Science, and Technology of Japan (to Y. N.).

REFERENCES

1 Folkman J. Tumor angiogenesis: therapeutic implications. *N Eng J Med* 1971; **285**: 1182–1186.
2 Dvorak HF, Brown LF, Detmar M, Dvorak AM. Vascular permeability factor/vascular endothelial growth factor, microvascular hyperpermeability, and angiogenesis. *Am J Pathol* 1995; **146**: 1029–1239.
3 Kligman LH. Symposium on models for the study of human photoaging: American Society for Photobiology. *Photochem Photobiol* 1989; **50**: 903–905.
4 Yano K, Oura H, Detmar M. Targeted overexpression of the angiogenesis inhibitor thrombospondin-1 in the epidermis of transgenic mice prevents ultraviolet-B-induced angiogenesis and cutaneous photo-damage. *J Invest Dermatol* 2002; **118**: 800–805.
5 Yano K, Kadoya K, Kajiya K, Hong YK, Detmar M. Ultraviolet B irradiation of human skin induces an angiogenic switch that is mediated by upregulation of vascular endothelial growth factor and by downregulation of thrombospondin-1. *Br J Dermatol* 2005 (Jan); **152** (1): 115–121.
6 Kramer M, Sachsenmaier C, Herrlich P, Rahmsdorf HJ. UV irradiation-induced interleukin-1 and basic fibroblast growth factor synthesis and release mediate part of the UV response. *J Biol Chem* 1993; **268**: 6734–6741.
7 Strickland I, Rhodes LE, Flanagan BF, Friedmann PS. TNF-alpha and IL-8 are upregulated in the epidermis of normal human skin after UVB exposure: correlation with neutrophil accumulation and E-selectin expression. *J Invest Dermatol* 1997; **108**: 763–768.
8 Bielenberg DR, Bucana CD, Sanchez R, Donawho CK, Kripke ML, Fidler IJ. Molecular regulation of UVB-induced cutaneous angiogenesis. *J Invest Dermatol* 1998; **111**: 864–872.
9 Hirakawa S, Fujii S, Kajiya K, Yano K, Detmar M. Vascular endothelial growth factor promotes sensitivity to ultraviolet B-induced cutaneous photodamage. *Blood* 2005; **105**: 2392–2399.
10 Oike Y, Ito Y, Maekawa H *et al.* Angiopoietin-related growth factor (AGF) promotes angiogenesis. *Blood* 2004; **103**: 3760–3765.
11 Oike Y, Akao M, Yasunaga K *et al.* Angiopoietin-related growth factor antagonizes obesity and insulin resistance. *Nat Med* 2005; **11**: 400–408.
12 Hato T, Tabata M, Oike Y. The role of angiopoietin-like proteins in angiogenesis and metabolism. *Trends Cardiovasc Med* 2008 (Jan); **18** (1): 6–14.
13 Oike Y, Yasunaga K, Ito Y *et al.* Angiopoietin-related growth factor (AGF) promotes epidermal proliferation, remodeling, and regeneration. *Proc Natl Acad Sci USA* 2003; **100**: 9494–9499.
14 Kajiya K, Hirakawa S, Detmar M. Vascular endothelial growth factor-A mediates ultraviolet B-induced impairment of lymphatic vessel function. *Am J Pathol* 2006; **169**: 1496–1503.
15 Hirakawa S, Detmar M. New insights into the biology and pathology of the cutaneous lymphatic system. *J Dermatol Sci* 2004 (Jun); **35** (1): 1–8.
16 Kajiya K, Sawane M, Huggenberger R, Detmar M. Activation of the VEGFR-3 pathway by VEGF-C attenuates UVB-induced edema formation and skin inflammation by promoting lymphangiogenesis. *J Invest Dermatol* 2009; **129**: 1292–1298.
17 Tabata M, Kadomatsu T, Fukuhara S *et al.* Angiopoietin-like protein 2 promotes chronic adipose tissue inflammation and obesity-related systemic insulin resistance. *Cell Metab* 2009; **10**: 178–188.
18 Hirakawa S, Kodama S, Kunstfeld R, Kajiya K, Brown LF, Detmar M. VEGF-A induces tumor and sentinel lymph node lymphangiogenesis and promotes lymphatic metastasis. *J Exp Med* 2005; **201**: 1089–1099.
19 Hirakawa S, Detmar M, Kerjaschki D *et al.* Nodal lymphangiogenesis and metastasis: role of tumor-induced lymphatic vessel activation in extramammary Paget's disease. *Am J Pathol* 2009; **175**: 2235–2248.
20 Detmar M, Brown LF, Schön MP *et al.* Increased microvascular density and enhanced leukocyte rolling and adhesion in the skin of VEGF transgenic mice. *J Invest Dermatol* 1998; **111**: 1–6.
21 Urano T, Ito Y, Akao M *et al.* Angiopoietin-related growth factor enhances blood flow via activation of the ERK1/2-eNOS-NO pathway in a mouse hind-limb ischemia model. *Arterioscler Thromb Vasc Biol* 2008; **28**: 827–834.
22 Kajiya K, Detmar M. An important role of lymphatic vessels in the control of UVB-induced edema formation and inflammation. *J Invest Dermatol* 2006; **126**: 919–921.

Naoki Sasaki[1]
Mika Shinjo[1]
Satoshi Hirakawa[2]
Masahiro Nishinaka[3]
Yo Tanaka[3]
Kazuma Mawatari[3,4]
Takehiko Kitamori[3,4]
Kae Sato[1,4]

[1]Department of Chemical and Biological Sciences, Faculty of Science, Japan Women's University, Mejirodai, Bunkyo-ku, Tokyo, Japan
[2]Department of Dermatology, Hamamatsu University School of Medicine, Handayama, Higashi-ku, Hamamatsu, Shizuoka, Japan
[3]Department of Applied Chemistry, Graduate School of Engineering, The University of Tokyo, Hongo, Bunkyo-ku, Tokyo, Japan
[4]Core Research for Evolutional Science and Technology (CREST), Japan Science and Technology Agency, Kawaguchi, Saitama, Japan

Received December 14, 2011
Revised March 8, 2012
Accepted March 13, 2012

Research Article

A palmtop-sized microfluidic cell culture system driven by a miniaturized infusion pump

A palmtop-sized microfluidic cell culture system is presented. The system consists of a microfluidic device and a miniaturized infusion pump that possesses a reservoir of culture medium, an electrical control circuit, and an internal battery. The footprint of the system was downsized to 87 × 57 mm, which is, to the best of our knowledge, the smallest integrated cell culture system. Immortalized human microvascular endothelial cells (HMEC-1) and human umbilical vein endothelial cells (HUVEC) were cultured in the system. HMEC-1 in the system proliferated at the same speed as cells in a microchannel perfused by a syringe pump and cells in a culture flask. HUVEC in the system oriented along the direction of the fluid flow. Claudin-5, a tight junction protein, was localized along the peripheries of the HUVEC. We expect that the present system is applicable to various cell types as a stand-alone and easy-to-use system for microfluidic bioanalysis.

Keywords:
Endothelial cells / Orientation / Perfusion culture / Proliferation / Tight junctions
DOI 10.1002/elps.201100691

1 Introduction

Microfluidic devices are among the attractive platforms for cell separation, cell culture, and cell-based assays [1, 2]. For example, microfluidic devices have been utilized for hydrodynamic [3] and acoustophoretic [4] separation of cells. On the other hand, cell cultures and subsequent assay of cells in a microchannel have also been studied. The size of a microchannel is smaller than that of a cell culture flask, and the number of cells and amount of reagents utilized can therefore be reduced. Moreover, multiple microchannels and microchambers can be easily fabricated on a single device [5], and various applications such as fast and high throughput analyses by parallelization are expected.

Various types of cells have been cultured on microfluidic devices, such as endothelial cells located at the inner surface of blood vessels [6]. The size of the microchannel is comparable to that of blood vessels, and shear stress due to fluid flow is applied to the endothelial cells cultured in the microchannel. In fact, a number of microfluidic devices for vascular research have been reported. The devices have been applied to various experiments, including cell culture [7–10], cell adhesion assay [11, 12], shear stress response analysis [13–21], permeability measurement [22, 23], and transendothelial electric resistance (TEER) measurement [24, 25]. Another example of a cell cultured on microfluidic devices is the osteoblastic cell [26, 27]. The cell is responsive to shear stress due to fluid flow, which is easily controlled by channel dimensions and flow velocity. We have also developed cell-based microfluidic devices [28], and have reported a leukocyte adhesion assay on endothelial cells [29], recovery of cultured endothelial cells from a separable microfluidic device [30], and the automated long-term monitoring of alkaline phosphatase activity of osteoblastic cells [31].

Pumping of fluids into a microchannel is important for cell-based microfluidic devices. For example, it is necessary to pump medium for a perfusion culture and to introduce reagents for assays. Various pumping methods for cell-based microfluidic devices have been reported. Pumping by hydrostatic pressure is simple and has been utilized by various

Correspondence: Professor Kae Sato, Department of Chemical and Biological Sciences, Faculty of Science, Japan Women's University, 2-8-1 Mejirodai, Bunkyo-ku, Tokyo 112-8681, Japan
E-mail: satouk@fc.jwu.ac.jp
Fax: +81-3-5981-3661

Abbreviations: HMEC-1, immortalized human microvascular endothelial cells; **HUVEC**, human umbilical vein endothelial cells; **TEER**, transendothelial electric resistance

Colour Online: See the article online to view Fig. 5 in colour.

studies [8,11,13]. However, the pumping can induce only continuous flow. In contrast, a computer-controlled pump can induce various types of flow, including continuous flow and pulsatile flow, at various flow rates. Both a syringe pump and a peristaltic pump have been utilized for cell-based microfluidic devices. However, the commercially available pumps are generally larger than microfluidic devices, an aspect that limits downsizing of the whole system. An integrated culture system driven by a peristaltic pump has been reported [32], but it requires a large medium reservoir and a large motor controller compared to the device. Microfabricated peristaltic pumps have been utilized to analyze secreted molecules from cells [33] and to culture cells in microchambers in an automated manner [34]. However, these systems require additional valves and tubes to control the pumps, and the structure of the microfluidic devices becomes complex. A palm-sized cell culture system driven by Braille pins has been reported [35], but it requires external power supply for long-term culture (>2 h).

In this paper, we present a palmtop-sized, stand-alone cell culture system that consists of a microfluidic device and a miniaturized infusion pump. All the required components are integrated into the system, and there is therefore no need for tubes or electrical connections from outside the system. As a result, the footprint of the system can be downsized to 87 × 57 mm. We apply the system to culture both immortalized and normal endothelial cells in a microchannel. Then, we evaluate the culture in terms of proliferation rate, cell orientation under fluid flow, and expression of tight junction proteins. Control experiments are conducted with a microfluidic device and a syringe pump as examples of conventional microfluidic cell culture systems.

2 Materials and methods

2.1 Cells and culture procedures

Immortalized human microvascular endothelial cells (HMEC-1) [36] and human umbilical vein endothelial cells (HUVEC; Lonza, Basel, Switzerland) were selected as representatives of endothelial cell lines and normal human endothelial cells, respectively. HMEC-1 was cultured in a 25-cm^2 cell culture flask (353014, Becton, Dickinson and Company, Franklin Lakes, NJ, USA). The cells were grown in MCDB 131 (Invitrogen, Carlsbad, CA, USA) supplemented with 30% FBS (Invitrogen), 1×GlutaMAX™-I Supplement (Invitrogen), 13 μg mL^{-1} Hydrocortisone (Sigma-Aldrich, St. Louis, MO, USA), and 10 ng mL^{-1} epidermal growth factor (Sigma-Aldrich). HUVEC was cultured in a 25 cm^2 cell culture flask (3289, Corning, NY, USA). The cells were grown in EBM™-2 (Lonza) supplemented with EGM™-2 BulletKit (Lonza). All reported experiments utilized cells between passages 3 and 8.

Once cells reached confluence, the medium in a cell culture flask was aspirated. The cells were rinsed with 5 mL of PBS (TAKARA BIO, Shiga, Japan) and then treated with 500 μL of TrypLE™ Express (Invitrogen). After the cells were detached from the surface of the flask, 1 mL of fresh medium was added, and the obtained cell suspension was added to 4 mL of fresh medium in a 15-mL conical tube. The tube was centrifuged at 1200 rpm for 3 min and the supernatant was aspirated. Finally, the cells were resuspended in the medium at the required concentration.

2.2 Microfabrication

Microfluidic devices were fabricated using standard microfabrication techniques [37]. A negative master for the molding of PDMS was fabricated on a glass slide (S1226, Matsunami Glass, Osaka, Japan) with photoresist (SU-8 50, MicroChem, Newton, MA, USA). The master contained four I-shaped convex patterns, which gave recessed microchannel patterns (300 μm width, 67 μm depth, 20 mm length) to the PDMS part (2 mm thickness) after the molding. The surface of the master was passivated by coating with a fluoropolymer (INT-332VE, Noda Screen, Aichi, Japan). A prepolymer of PDMS (SILPOT 184, Dow Corning, Midland, MI, USA) was poured onto the master with a frame for holding the prepolymer. The prepolymer was cured in an oven at 65°C for 60 min, and the cured PDMS was peeled off from the master, bonded to a virgin glass slide, and cured again at 100°C for 60 min. Through -holes for tubes were punched at the end of the microchannel patterns on the PDMS part using a metal pipe. The PDMS part was then cut into four parts, each of which had the microchannel. Silicone tubes (0.5 mm id, 1.0 mm od, AS ONE, Osaka, Japan) or PTFE tubes (0.46 mm id, 0.92 mm od, NICHIAS, Tokyo, Japan) were glued to the through-holes with the prepolymer at 65°C for 60 min. The PDMS part with the tubes was sterilized in an autoclave at 121°C for 20 min, bonded to the bottom part of a 35-mm cell culture dish (Asahi glass, Tokyo, Japan), and kept in a clean bench until cell culture experiments.

2.3 Microfluidic cell culture systems

Figure 1A and B show microfluidic cell culture systems driven by a syringe pump (model 210, KD Scientific, Holliston, MA, USA). HMEC-1 was cultured in the system shown in Fig. 1A. One of the silicone tubes was connected to a 1-mL syringe (Terumo, Tokyo, Japan) via a metal pipe (0.33 mm id, 0.63 mm od, Nonaka Rikaki, Tokyo, Japan), a perfluoroalkoxy capillary (0.1 mm id, 0.3 mm od, Iwase, Kanagawa, Japan), and a needle (0.33 mm id, 0.63 mm od, Nonaka Rikaki). The other tube was connected to a capillary via a pipe. HUVEC was cultured in the system shown in Fig. 1B. One of the PTFE tubes was connected to a syringe via a bubble trap, a capillary, and a needle. The bubble trap was fabricated in accordance with details provided in the literature [38]. Two TYGON™ tubes (0.79 mm id, 2.38 mm od, Saint-Gobain K.K., Tokyo, Japan) and another TYGON tube (2 mm id, 4 mm od, Saint-Gobain K.K.) were used to compose the trap.

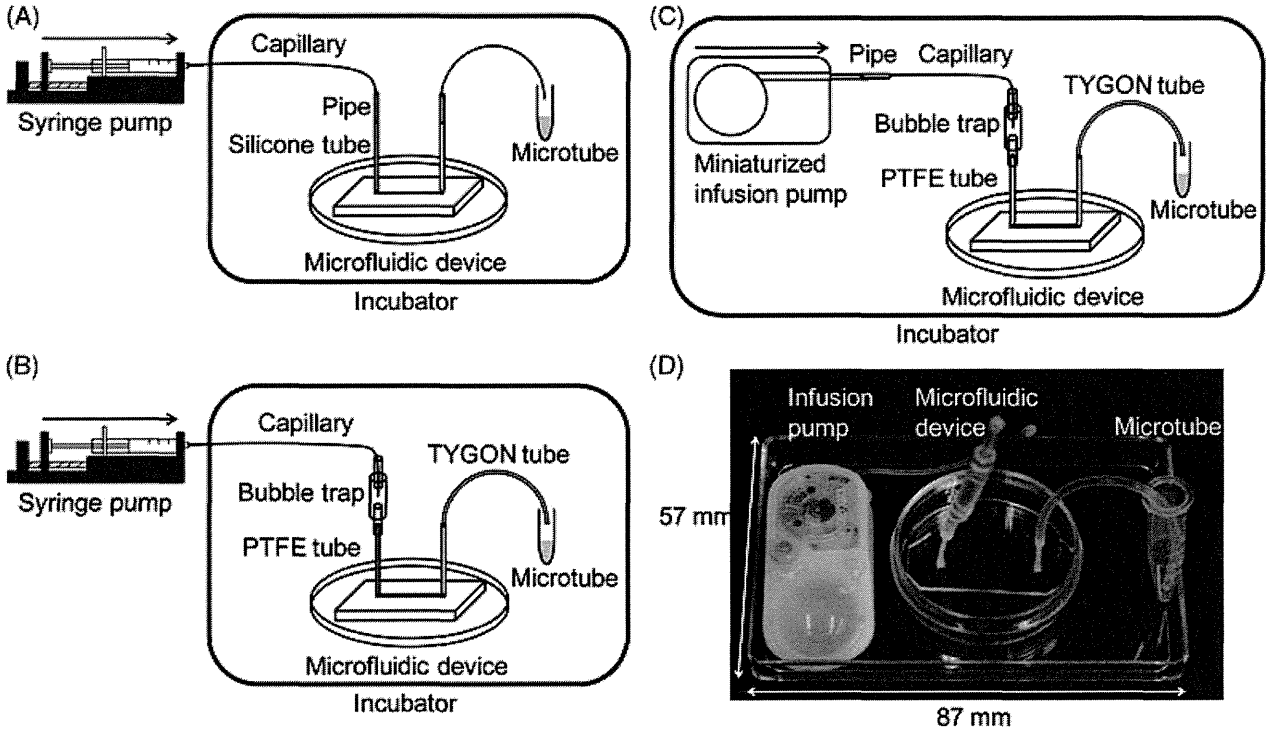

Figure 1. Microfluidic cell culture systems. (A–C) Schematic illustrations of microfluidic cell culture system. (A) A system with a syringe pump. (B) A system with a syringe pump and a bubble trap. (C) A palmtop-sized culture system with a miniaturized infusion pump and a bubble trap. (D) Photograph of the palmtop-sized microfluidic cell culture system.

The other PTFE tube on the microfluidic device was also connected to a TYGON tube. In the palmtop-sized microfluidic cell culture system shown in Fig. 1C, a miniaturized infusion pump (SMP101-L, Primetech, Tokyo, Japan) was used instead of the syringe pump shown in Fig. 1B. The components of the systems were glued with epoxy adhesive as required.

2.4 Cell culture in a microchannel

All the tubes, pipes, and capillaries used in this study were sterilized in an autoclave at 121°C for 20 min. Medium for cell culture was incubated in an incubator for 30 min prior to experiments to equilibrate the concentration of CO_2 in the medium with that in the incubator. Microfluidic devices were degassed in a vacuum desiccator (PC-150K, Sanplatec, Osaka, Japan) connected to a vacuum pump (DAP-6D, Ulvac, Kanagawa, Japan) at 10 kPa for 30 min to prevent air bubbles remaining in the microchannels [39].

A suspension of cells was prepared at a cell concentration of 5×10^6 cells mL^{-1} and then introduced into a microchannel manually or by a syringe pump. Capillaries were then pinched by clips to stop the flow in the microchannel. The microfluidic device was wrapped with a wet lint-free wiper (BEMCOT™ M-1, Asahi Kasei, Tokyo, Japan) in plastic wrap to humidify the device. The microfluidic device was incubated at 37°C under an atmosphere of 5% CO_2 and 95% air for 5 h to allow cells to adhere to the bottom of the channel. The medium was then infused into the channel at 6.0 μL h^{-1} by the syringe pump placed outside the incubator (Fig. 1A and B) or the miniaturized infusion pump placed inside the incubator (Fig. 1C).

Shear stress during the culture was estimated as follows. Time-averaged shear stress τ in a rectangular microchannel is written as [40]:

$$\tau = \frac{2\mu Q}{wh^2}\left(\frac{m+1}{m}\right)(n+1) \quad (1)$$

where μ is the viscosity of the medium, Q is the volume flow rate, h is the height of the microchannel, w is the width of the microchannel, and m and n are empirical constants, with $m = 1.7 + 0.5(h/w)^{-1.4}$ and $n = 2$ for aspect ratios $h/w < 1/3$. As described previously [29], μ was assumed to be the same as that of water at 37°C, and estimated to be 7.0×10^{-3} g cm^{-1} s^{-1}. Using the μ value, a h of 67 μm, w of 300 μm, Q of 6.0 μL h^{-1} and Eq. 1, we obtained 0.061 dyn cm^{-2} as the time-averaged shear stress in the microchannel.

The miniaturized pump creates intermittent flow because of its peristaltic mechanism. Therefore, we measured instantaneous volume flow rate in a separate experiment and estimated shear stress (see Supporting information). The maximum instantaneous volume flow rate was 16.3 μL h^{-1}, and we obtained 0.17 dyn cm^{-2} as the maximum instantaneous shear stress.

The cultured cells were observed using an inverted microscope (IX71, Olympus, Tokyo, Japan) equipped with a CCD camera (Rolera XR, QImaging, Surrey, BC, Canada).

Phase-contrast images of HMEC-1 and HUVEC were taken at 102 h and 50 h, respectively, after introduction of the cell suspension.

2.5 Evaluation of proliferation rate

In macroscale experiments, 250 μL of a HMEC-1 suspension at a cell concentration of 4×10^5 cells mL^{-1} was added to 5 mL of fresh medium in a cell culture flask, and the cells were cultured under a static condition. In microscale experiments, microfluidic devices were degassed as described in the previous section. The medium was introduced into the microchannel at 1200 μL h^{-1} by a syringe pump. A suspension of HMEC-1 at a cell concentration of 5×10^6 cells mL^{-1} was then introduced into the microchannel at 600 μL h^{-1}, and the microfluidic devices were incubated in the CO_2 incubator for 4 h. Finally, the medium was pumped into the channel by the syringe pump or a miniaturized infusion pump at 6.0 μL h^{-1}. The cultured cells were observed as described in the previous section. Phase-contrast images of HMEC-1 were taken at 4 h (just before pumping medium), 28 h, 53 h, 83 h, 102 h, and 129 h after introduction of the cell suspension.

2.6 Evaluation of orientation

The orientation of HUVEC was evaluated in accordance with details provided in the literature [16]. Briefly, the angle of orientation was defined as the angle between the long axis of the cell and the direction of flow. Therefore, the angle of a cell that is completely oriented parallel to the microchannel is regarded as 0°, whereas the angle of a cell that is completely oriented perpendicular to the microchannel is regarded as 90°.

2.7 Immunofluorescent staining

HUVEC cultured in a microchannel were immunostained for Claudin-5, a transmembrane protein that is involved in tight junctions between endothelial cells [41]. After 50 h in culture, HUVEC was fixed with methanol, rinsed with PBS, blocked with PBS containing 1% BSA (Wako Pure Chemical Industries, Osaka, Japan) for 30 min, rinsed with PBS three times for 5 min each, and then reacted with 10 μg mL^{-1} anti-Claudin-5 antibody (ab53765, abcam, Cambridge, UK) for 12 h at 4°C. The cells were then rinsed with PBS three times for 5 min each, reacted with 6.7 μg mL^{-1} Alexa Fluor™ 555 goat anti-rabbit IgG antibody (A-21429, Invitrogen) for 30 min at room temperature, and rinsed with PBS three times for 5 min each. The nuclei of cells were counterstained with Dapi-Fluoromount-G™ (SouthernBiotech, Birmingham, AL, USA). Fluorescence images were taken using the same microscope described in Section 2.4 equipped with a 100-W high-pressure mercury lamp, a 20× objective lens (NA 0.40), and a cooled CCD camera (ORCA-R2, Hamamatsu Photonics, Hamamatsu, Japan). For Claudin-5 observation, a dichroic mirror block (U-MWIG3, excitation 530–550 nm and emission >575 nm) was used. For the observation of nuclei, another dichroic mirror block (U-MNUA2, excitation 360–370 nm and emission 420–460 nm) was used. The images were processed using image analysis software (Image J 1.45f, National Institutes of Health, MD, USA).

3 Results and discussions

3.1 Palmtop-sized microfluidic cell culture system

Figure 1D shows a photograph of the palmtop-sized microfluidic cell culture system. The system consists of a miniaturized infusion pump, a microfluidic device, a microtube, and tubes and capillaries that connect the components of the system. A reservoir (900 μL) of culture medium and an electrical control circuit are integrated into the pump (44 mm length, 22 mm width, 10 mm height, 7 g weight). The reservoir is connected to a rubber tube in the pump, and the tube is pushed by seven pins in the pump in a sequential manner. Therefore, the medium is pumped in a peristaltic manner. The range of volume flow rate is 1.0~30.0 μL h^{-1}. The pump is programmable, and we can configure up to ten discrete infusion steps. The pump is commercially available at low cost (¥25 000 per pump). The pump is disposable since it is an implantable pump for small laboratory animals, but should be reusable in our system if it is sterilized with appropriate solutions (e.g., 70% ethanol). In addition, the pump is powered by an internal battery, and therefore no cables or tubes are required from outside the system. As a result, the footprint of the whole system was reduced to 87 × 57 mm, which is, to the best of our knowledge, the smallest integrated cell culture system. The system can be placed in an incubator for culture and on a microscope for observation without detaching any electrical or fluidic connections from the system.

3.2 Culture of endothelial cells

Figure 2 shows typical images of HMEC-1 and HUVEC cultured in a microchannel. Both types of cells reached confluence in the microchannel, whether the channel was perfused by a syringe pump (Fig. 2A and C) or a miniaturized infusion pump (Fig. 2B and D). Therefore, both cell lines and normal cells reached confluence in the palmtop-sized cell culture system. HMEC-1 was not oriented to a specific direction, whereas HUVEC was oriented to the direction of the channel. The orientation of HUVEC is further discussed in Section 3.4.

We also observed air bubbles in the systems in some experiments. HMEC-1 was successfully cultured in the system shown in Fig. 1A. In contrast, when HUVEC was cultured in the system shown in Fig. 1A, air bubbles flowed into the channel and detached the cells from the surface of the channel (data not shown). Such issues were solved by placing

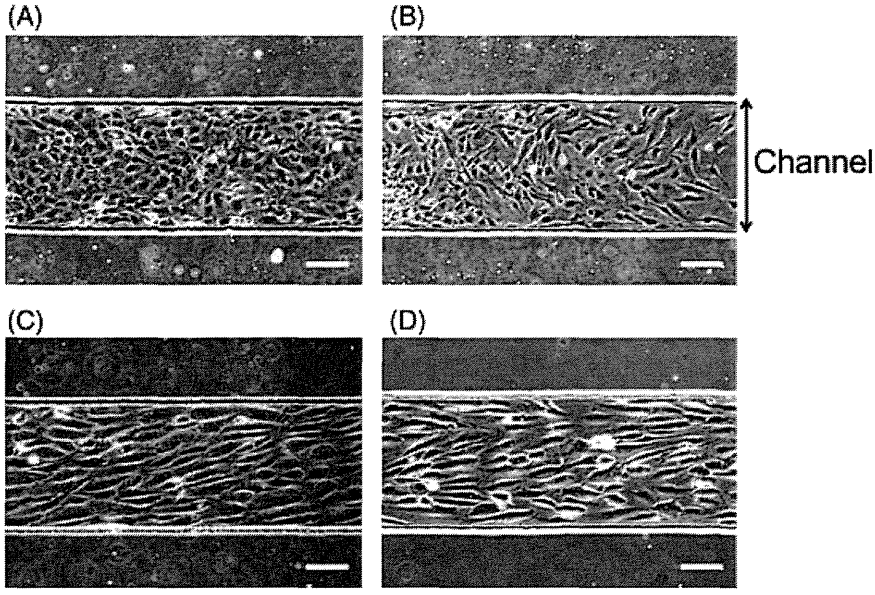

Figure 2. Phase-contrast images of (A, B) HMEC-1 and (C, D) HUVEC cultured in a microchannel. The cells were cultured with (A, C) a syringe pump and (B, D) a miniaturized infusion pump. Scale bar: 100 μm.

the bubble trap at the upstream point of the microchannel, as shown in Fig. 1B and C.

3.3 Growth rate of endothelial cells

Figure 3 shows the growth curve of HMEC-1 under three different culture procedures: static culture in a culture flask, perfusion culture in a microchannel with a syringe pump, and perfusion culture in a microchannel with a miniaturized infusion pump. In a culture flask, the cell density was 96 ± 28 cells mm^{-2} at the culture time of 4 h. The density then increased with time, and reached (1.4 ± 0.3) × 10^3 cells mm^{-2} at 102 h. Afterward, the density was almost constant, which meant the cells reached confluence at 102 h. In a microchannel perfused by a syringe pump, the cell density was (1.4 ± 0.4) × 10^2 cells mm^{-2} at 4 h and reached (1.1 ± 0.1) × 10^3 cells mm^{-2} at 102 h. In a microchannel perfused by a miniaturized infusion pump, the cell density was (1.5 ± 0.4) × 10^2 cells mm^{-2} at 4 h and reached (1.2 ± 0.1) × 10^3 cells mm^{-2} at 102 h. Clearly, the cell densities at the culture time of 4 h and 102 h in the aforementioned culture procedures were almost the same, and hence the proliferation rates of cells were also the same. Therefore, HMEC-1 cultured with the miniaturized infusion pump proliferated in a way similar to cells cultured with the syringe pump and in a culture flask.

3.4 Orientation

Figure 4 shows a histogram of the orientation angle of HUVEC under the different culture procedures. Under static culture in a culture flask, the orientation angle of HUVEC was random: the averaged orientation angle was 43.3 ± 25.1°,

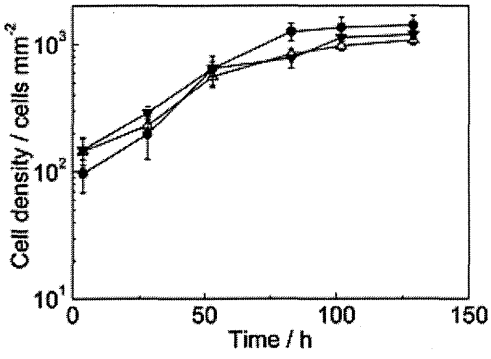

Figure 3. Growth curve of HMEC-1 under three different culture procedures: static culture in a culture flask (filled circles), perfusion culture in a microchannel with a syringe pump (open triangles), and perfusion culture in a microchannel with a miniaturized infusion pump (filled inverted triangles). The error bars indicate ±1SD of three experiments.

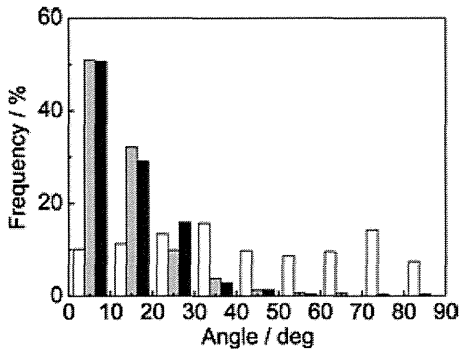

Figure 4. Histogram of orientation angle of HUVEC under three different culture procedures: static culture in a culture flask (white), perfusion culture in a microchannel with a syringe pump (gray), and perfusion culture in a microchannel with a miniaturized infusion pump (black). Culture time: 50 h. Data were taken from three experiments.

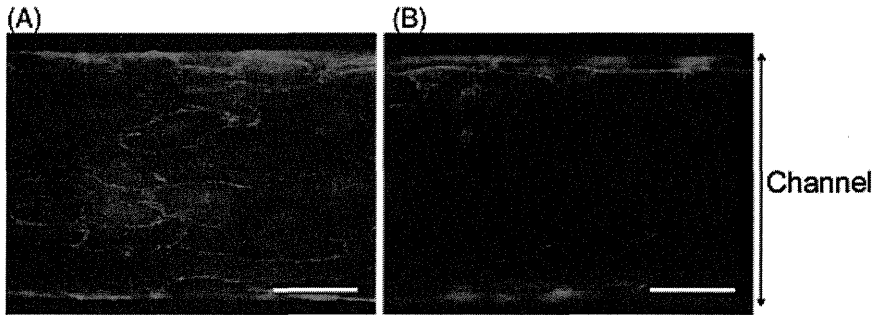

Figure 5. Immunofluorescence micrographs of HUVEC in a microchannel. Cells were immunostained for Claudin-5 (red, a marker of tight junctions). Nuclei of cells were counterstained with Dapi-Fluoromount-G (blue). (A) HUVEC cultured with a syringe pump. (B) HUVEC cultured with a miniaturized infusion pump. Scale bar: 100 μm.

which is close to the theoretical value of the averaged orientation angle for randomly oriented cells (45°). In contrast, the orientation angles of HUVEC cultured in microchannels were around zero: the averaged orientation angle of HUVEC cultured with a syringe pump and with a miniaturized infusion pump was 12.4 ± 12.0° and 12.1 ± 9.6°, respectively. Therefore, HUVEC was oriented to the direction along the channel. This result is consistent with previous reports concerning the orientation of HUVEC under continuous flow in a microchannel [13, 15].

3.5 Tight junctions

Tight junctions are a type of the intercellular junction, which represent the major transport pathway across the endothelium [42]. The presence of tight junctions between endothelial cells cultured in a microchannel has been demonstrated by TEER measurement [24]. However, the presence of tight junction proteins at the junctions has not been confirmed. Figure 5 shows immunofluorescence images of HUVEC in a microchannel. Claudin-5, the major transmembrane component of endothelial tight junctions, was localized along the cell peripheries as previously reported [43, 44], regardless of the type of pump used in the experiment. Therefore, the presence of tight junction proteins was confirmed with both types of pumps.

4 Concluding remarks

We have developed a palmtop-sized microfluidic cell culture system driven by a miniaturized infusion pump. Both HMEC-1 and HUVEC reached confluence in the system. HMEC-1 in the system proliferated with a rate similar to that of cells cultured with a syringe pump and in a culture flask. HUVEC was oriented in the microchannel regardless of the type of pump used in the experiment. The presence of tight junction proteins between the endothelial cells was, for the first time, directly confirmed by immunostaining of Claudin-5. We expect that the palmtop-sized microfluidic cell culture system is applicable to various cell types as a stand-alone and easy-to-use system for microfluidic bioanalysis.

The authors thank Prof. R. Shimada (Department of Mathematical and Physical Sciences, Faculty of Science, Japan Women's University) for her assistance with microfabrication. This work was partially supported by the JGC Corporation and JST CREST (Core Research for Evolutional Science & Technology).

The authors have declared no conflict of interest.

5 References

[1] Lenshof, A., Laurell, T., *Chem. Soc. Rev.* 2010, *39*, 1203–1217.

[2] Wu, M.-H., Huang, S.-B., Lee, G.-B., *Lab Chip* 2010, *10*, 939–956.

[3] Yamada, M., Kano, K., Tsuda, Y., Kobayashi, J., Yamato, M., Seki, M., Okano, T., *Biomed. Microdev.* 2007, *9*, 637–645.

[4] Petersson, F., Åberg, L., Swärd-Nilsson, A.-M., Laurell, T., *Anal. Chem.* 2007, *79*, 5117–5123.

[5] Hung, P. J., Lee, P. J., Sabounchi, P., Lin, R., Lee, L. P., *Biotechnol. Bioeng.* 2005, *89*, 1–8.

[6] Young, E. W. K., Simmons, C. A., *Lab Chip* 2010, *10*, 143–160.

[7] Fidkowski, C., Kaazempur-Mofrad, M. R., Borenstein, J., Vacanti, J. P., Langer, R., Wang, Y., *Tissue Eng.* 2005, *11*, 302–309.

[8] Golden, A. P., Tien, J., *Lab Chip* 2007, *7*, 720–725.

[9] Shin, M., Matsuda, K., Ishii, O., Terai, H., Kaazempur-Mofrad, M., Borenstein, J., Detmar, M., Vacanti, J. P., *Biomed. Microdev.* 2004, *6*, 269–278.

[10] Lindström, S., Mori, K., Ohashi, T., Andersson-Svahn, H., *Electrophoresis* 2009, *30*, 4166–4171.

[11] Chrobak, K. M., Potter, D. R., Tien, J., *Microvasc. Res.* 2006, *71*, 185–196.

[12] Song, J. W., Cavnar, S. P., Walker, A. C., Luker, K. E., Gupta, M., Tung, Y.-C., Luker, G. D., Takayama, S., *PLoS ONE* 2009, *4*, e5756.

[13] Tkachenko, E., Gutierrez, E., Ginsberg, M. H., Groisman, A., *Lab Chip* 2009, *9*, 1085–1095.

[14] Chau, L., Doran, M., Cooper-White, J., *Lab Chip* 2009, *9*, 1897–1902.

[15] van der Meer, A. D., Poot, A. A., Feijen, J., Vermes, I., *Biomicrofluidics* 2010, *4*, 011103.

